

Supplementary Information to:

Rational design of DNA-actuated enzyme nanoreactors guided by single molecule analysis

Soma Dhakal¹, Matthew R. Adendorff^{2,1}, Minghui Liu^{3,4,1}, Hao Yan^{3,4,*}, Mark Bathe^{2,*}, Nils G. Walter^{1,*}

¹Department of Chemistry, Single Molecule Analysis Group, University of Michigan, Ann Arbor, MI 48109, USA. ²Department of Biological Engineering, Laboratory for Computational Biology & Biophysics, Massachusetts Institute of Technology, Cambridge, MA 02139, USA. ³Center for Molecular Design and Biomimetics, The Biodesign Institute, ⁴Department of Chemistry and Biochemistry, Arizona State University, Tempe, AZ 85287, USA.

¹These authors contributed equally to this work.

*Corresponding authors: N. G. W. (nwalter@umich.edu); M. B. (mark.bathe@mit.edu); H. Y. (hao.yan@asu.edu);

Table of contents:

Section 1: DNA sequences, assembly, and bulk characterization of DNA tweezers.....S3

Section 2: Single molecule FRET (smFRET) characterization of DNA tweezers.....S14

Section 3: Atomic force microscopy (AFM) imaging of DNA tweezers.....S26

Section 4: Molecular dynamics (MD) simulation of DNA tweezers.....S30

Section 5: Bulk measurement of tweezer-scaffolded G6pDH activity.....S35

Section 6: Single molecule measurement of tweezer-scaffolded G6pDH activity.....S38

References.....S43

Section 1: DNA sequences, assembly, and bulk characterization of DNA tweezers

Table S1. Sequences of original hairpin (3T3bp), hairpin removed (0T0bp and 1T0bp), and hairpin redesigned (1T3bp, 1T4bp and 1T5bp) DNA tweezers. Each tweezer design contains one of the T7 strands (shaded), which dictates the name of the tweezer (3T3bp tweezer has a 3-nt spacer (red) and a stem region of 3bp length (blue), for example). Strand TB1 is labeled with biotin. Tweezers for bulk measurements were assembled with regular T3 and TP8 strands without fluorescent dyes, whereas these strands were fluorophore labeled for single molecule experiments. The 3' end of strand T9 is conjugated to the NAD⁺ molecule via a 20T linker. Protruding complementary sequences used to capture oligonucleotide-modified protein on the tweezer are highlighted in cyan and green.

Name	Sequence
TB1	TTTTTCGACCGAGCGTGAATTAGTGATCCGGAACTCGCGCAATGAACCTTTT/3BioTEG/
TP2	TTTTTCAGCTGGCCATCTAAGACTGAACTCGCACCCGCCGATAAGCTATGCGCTCTGCCGCTTTGGAGGG AGGG
T3	TTTTTAGGAGATGGCACGTTAATGAATAGTCTCCACTTGCATCCGAGATCCGAACTGCTGCC
T3-Cy3	Cy3 -TTTTTAGGAGATGGCACGTTAATGAATAGTCTCCACTTGCATCCGAGATCCGAACTGCTGCC
TB4	TTTTCGAGAGAAGGCTTGCCAGGTTACGTTTCGTACATCGTCTGAGTTTTT
T5	TTTTGGCAGCAGTTCAGGCCAGCTGATTTT
T6	TTTTGGTTCATTGCGGAGTTCAGTCTTAGATGGATCTCGGATGCAAGGCCTTCTCTCGTTTT
T7 (3T3bp)	GGTGCCGAGTTCGGATCACTAATTCATAGCTTATGCCGGCTTT TGCG TAAGACCCACAAT CGCTT ACTA TTCATTAACGTGTGTACGAACGTAACCTGGCAATGGAG
T7 (0T0bp)	GGTGCCGAGTTCGGATCACTAATTCATAGCTTATGCCGGCACTATTCAATTAACGTGTGTACGAACGTAAC CTGGCAATGGAG
T7 (1T0bp)	GGTGCCGAGTTCGGATCACTAATTCATAGCTTATGCCGGCT TT ACTATTCAATTAACGTGTGTACGAACGTA ACCTGGCAATGGAG
T7 (1T3bp)	GGTGCCGAGTTCGGATCACTAATTCATAGCTTATGCCGGCT TGCG TAAGACCCACAAT CGCT ACTATTCA TTAACGTGTGTACGAACGTAACCTGGCAATGGAG
T7 (1T4bp)	GGTGCCGAGTTCGGATCACTAATTCATAGCTTATGCCGGCT TGCGG TAAGACCCACAAT CCGCT ACTATT CATTAAACGTGTGTACGAACGTAACCTGGCAATGGAG
T7 (1T5bp)	GGTGCCGAGTTCGGATCACTAATTCATAGCTTATGCCGGCT TGCGGG TAAGACCCACAAT CCCGCT ACT ATTCATTAACGTGTGTACGAACGTAACCTGGCAATGGAG
TP8	TTTTGCGGCAGAGCGACGCTCGGTCGTTTGGAGGGAGGG
TP8-Cy5	Cy5 -TTTTGCGGCAGAGCGACGCTCGGTCGTTTGGAGGGAGGG
T9-20T	AACTCAGACGACCATCTCCTAATTTTTTTTTTTTTTTTTTTT/3AmMO/

Table S2. Sequences of the 1T4bp tweezer with redesigned HJ1 using iso-I (1T4bp-HJ1-iso-I) of Seeman's HJ J1.¹⁻³ Redesigned inner-core sequences are bolded and underlined.

Name	Sequence
TB1	TTTTCGACCGAGCGTGAATTAGTGATCCGGAACTCGCGCAATGAACCTTTT/3BioTEG/
TP2	TTTTTCAGCTGGCC <u>GAT</u> CTAAGACTGAACTCGCACCGCCGGCATAAGCTATGCGCTCTGCCGCTTT GGAGGGAGGG
T3-Cy3	Cy3-TTTTAGGAGATGGCACGTTAATGAATAGTCTCCACTTGCATCCGAGATC <u>CTAACTGCTGCC</u>
T4	TTTTCGAGAGAAGGCTTGCCAGGTTACGTTTCGTACATCGTCTGAGTTTTT
T5	TTTTGGCAGCAGTT <u>ACGGCC</u> AGCTGATTTT
T6	TTTTGGTTCATTGCGGAGTTCAGTCTTAGAT <u>TGGAT</u> CTCGGATGCAAGGCCTTCTCTCGTTTT
T7 (1T4bp)	GGTGCCGAGTTCGGATCACTAATTCATAGCTTATGCCGGCTGCGGTAAGACCCACAATCCGCTA CTATTCATTAACGTGTGTACGAACGTAACCTGGCAATGGAG
TP8-Cy5	Cy5-TTTTGCAGCAGAGCGACGCTCGGTCGTTTGGAGGGAGGG
Set	CGTGTGGTTGAGCGGATTGTGGGTCTTACCGCA
Fuel	TGCGGTAAGACCCACAATCCGCTCAACCACACG
T9-20T	AACTCAGACGACCATCTCCTAATTTTTTTTTTTTTTTTTTTT/3AmMO/

Table S3. Sequences of the 1T4bp tweezer with all five Holliday junctions (HJ1 to HJ5) redesigned based on iso-I of Seeman's HJ J1¹⁻³ (1T4bp-5HJs-iso-I), matching the 5'-3' direction of the core sequence with HJ1. Redesigned inner-core sequences are bolded and underlined.

Name	Sequence
TB1	TTTTTCGACCGAGCGG <u>GAA</u> ATTAGTGATCCGGAAC <u>TCGAG</u> CAATGAACCTTTT/3BioTEG/
TP2	TTTTTCAGCTGGCC <u>GAT</u> CTAAGACTGAACT <u>CT</u> CACCGCCGGCATAAGCTAT <u>CT</u> GTCTGCTGCCGCTTTGGAGGGAGGG
T3-Cy3	Cy3-TTTTAGGAGATG <u>GA</u> ACGTTAATGAATAGTCTCC <u>GAT</u> TGCATCCGAGATC <u>CT</u> AACTGCTGCC
T4	TTTTTCGAGAGAAGG <u>CT</u> TGCCAGGTTACGTTTCGTAC <u>CT</u> CGTCTGAGTTTTTTT
T5	TTTTGGCAGCAGTT <u>AC</u> GGCCAGCTGATTTT
T6	TTTTGGTTCATTGCT <u>TG</u> AGTTCAGTCTTAGAT <u>TG</u> GATCTCGGATGCAAT <u>TG</u> CCTTCTCTCGTTTT
T7 (1T4bp)	GGT <u>AC</u> GAGTTCGGATCACTAATT <u>TG</u> ATAGCTTATGCCGGCTGCGGTAAGACCCACAATCCGCTACTATTCATTAACGT <u>TG</u> GTACGAACGTAACCTGGCA <u>AC</u> GGAG
TP8-Cy5	Cy5-TTTTGC GGCAGAGC <u>AC</u> CGCTCGGTCGTTTGGAGGGAGGG
Set	CGTGTGGTTGAGCGGATTGTGGGTCTTACCGCA
Fuel	TGCGGTAAGACCCACAATCCGCTCAACCACAG
C3-T9-20T	AACTCAGACG <u>ACC</u> ATCTCCTAATTTTTTTTTTTTTTTTTTTT/3AmMO/
T3	TTTTTAGGAGATG <u>GA</u> ACGTTAATGAATAGTCTCC <u>GAT</u> TGCATCCGAGATC <u>CT</u> AACTGCTGCC
TP8	TTTTGCGGCAGAGC <u>AC</u> CGCTCGGTCGTTTGGAGGGAGGG

Table S4. Sequences of the 1T4bp tweezer with redesigned HJ1 using iso-II of Seeman's HJ J1¹⁻³ (1T4bp-HJ1-iso-II), a control design. Redesigned inner-core sequences are bolded and underlined.

Name	Sequence
TB1	TTTTCGACCGAGCGTGAATTAGTGATCCGGAACTCGCGCAATGAACCTTTT/3BioTEG/
TP2	TTTTTCAGCTGGCC <u>TGT</u> CTAAGACTGAACTCGCACCGCCGGCATAAGCTATGCGCTCTGCCGCTTT GGAGGGAGGG
T3-Cy3	Cy3-TTTTAGGAGATGGCACGTTAATGAATAGTCTCCACTTGCATCCGAGATC <u>ACA</u> ACTGCTGCC
T4	TTTTCGAGAGAAGGCTTGCCAGGTTACGTTTCGTACATCGTCTGAGTTTTT
T5	TTTTGGCAGCAGTT <u>GAG</u> CCAGCTGATTTT
T6	TTTTGGTTCATTGCGGAGTTCAGTCTTAGA <u>CT</u> GATCTCGGATGCAAGGCCTTCTCTCGTTTT
T7 (1T4bp)	GGTGCCGAGTTCGGATCACTAATTCATAGCTTATGCCGGCTGCGGTAAGACCCACAATCCGCTA CTATTCATTAACGTGTGTACGAACGTAACCTGGCAATGGAG
TP8-Cy5	Cy5-TTTTGCAGCAGAGCGACGCTCGGTCGTTTGGAGGGAGGG
Set	CGTGTGGTTGAGCGGATTGTGGGTCTTACCGCA
Fuel	TGCGGTAAGACCCACAATCCGCTCAACCACACG
T9-20T	AACTCAGACGACCATCTCCTAATTTTTTTTTTTTTTTTTTTT/3AmMO/

Table S5. Sequences of the isolated HJ1 (original 3T3bp tweezer) with a regular and a flipped labeling scheme for the FRET pair (Cy3/Cy5).

Name	Sequence (Labeling Scheme-I)
TP2	TTTTTCAGCTGGCCTATCTAAGACTG
T3Cy3	/5Cy3/ATCCGAGATCCGAACTGCTGCC
T5Biotin	/5BiotinTEG/TTTTGGCAGCAGTTCAGGCCAGCTGATTTT
T6Cy5	/5Cy5/CAGTCTTAGATGGATCTCGGAT
Name	Sequence (Labeling Scheme-II)
TP2Cy3	/5Cy3/TCAGCTGGCCTATCTAAGACTG
T3	ATCCGAGATCCGAACTGCTGCC
T5Biotin	/5BiotinTEG/TTTTGGCAGCAGTTCAGGCCAGCTGATTTT
T6Cy5	/5Cy5/CAGTCTTAGATGGATCTCGGAT

Table S6. Estimated extinction coefficients of all tweezers used in our measurements. The theoretical extinction coefficients were obtained by summing the extinction coefficients of all DNA strands (both double- and single-stranded DNAs) and protein/NAD⁺ components involved. G6pDH: $\epsilon_{260} \sim 61594 \text{ M}^{-1}\text{cm}^{-1}$; 6AE-NAD⁺: $\epsilon_{260} \sim 21000 \text{ M}^{-1}\text{cm}^{-1}$ (provided by Biolog, Hayward, CA, USA).

DNA Tweezer	Theoretical ϵ_{260} ($\text{M}^{-1} \text{cm}^{-1}$)
3T3bp (open)	4162384.9
1T3bp (open)	4105635.3
1T4bp (open)	4138847.2
1T5bp (open)	4174447.5
1T4bp-HJ1-iso-I (open)	4135293.4
1T4bp-5HJs-iso-I (open)	4139136.2
1T4bp-HJ1-iso-II (open)	4136108.6
3T3bp (close)	4003121.4
1T3bp (close)	3954125.0
1T4bp (close)	3971369.5
1T5bp (close)	3992879.8
1T4bp-HJ1-iso-I (close)	3967815.7
1T4bp-5HJs-iso-I (close)	3971658.5
1T4bp-HJ1-iso-II (close)	3968630.9
3T3bp (open)-G6pDH	4338484.7
1T3bp (open)-G6pDH	4281735.1
1T4bp (open)-G6pDH	4314947.0
1T5bp (open)-G6pDH	4350547.3
1T4bp-5HJs-iso-I (open)-G6pDH	4315236.0
3T3bp (close)-G6pDH	4179221.2
1T3bp (close)-G6pDH	4130224.8
1T4bp (close)-G6pDH	4147469.3
1T5bp (close)-G6pDH	4168979.6
1T4bp-5HJs-iso-I (close)-G6pDH	4147758.3

a

Hairpin Actuator	Sequence (5' to 3')
3T3bp	TTT GCG TAAGACCCACAAT CGCTTT
1T3bp	T GCG TAAGACCCACAAT CGCT
1T4bp	T GCGG TAAGACCCACAAT CCGCT
1T5bp	T GCGGG TAAGACCCACAAT CCCGCT

b

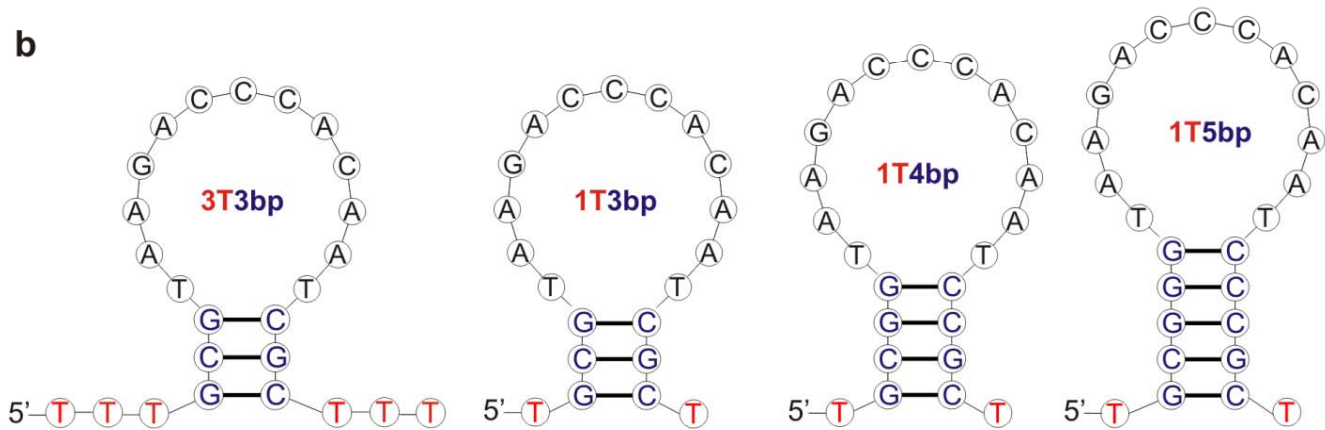


Fig. S1. mFold prediction of the hairpin-actuator secondary structure of the different tweezers. (a) Hairpin sequences used as inter-arm linkers in different tweezers. The single-stranded flanking spacer, the hairpin stem, and loop sequences are highlighted in red, blue and black, respectively. (b) mFold⁴ predicted folding of the DNA linker sequences (UNAFold Tool; Integrated DNA Technologies, Inc., Coralville, IA, USA).

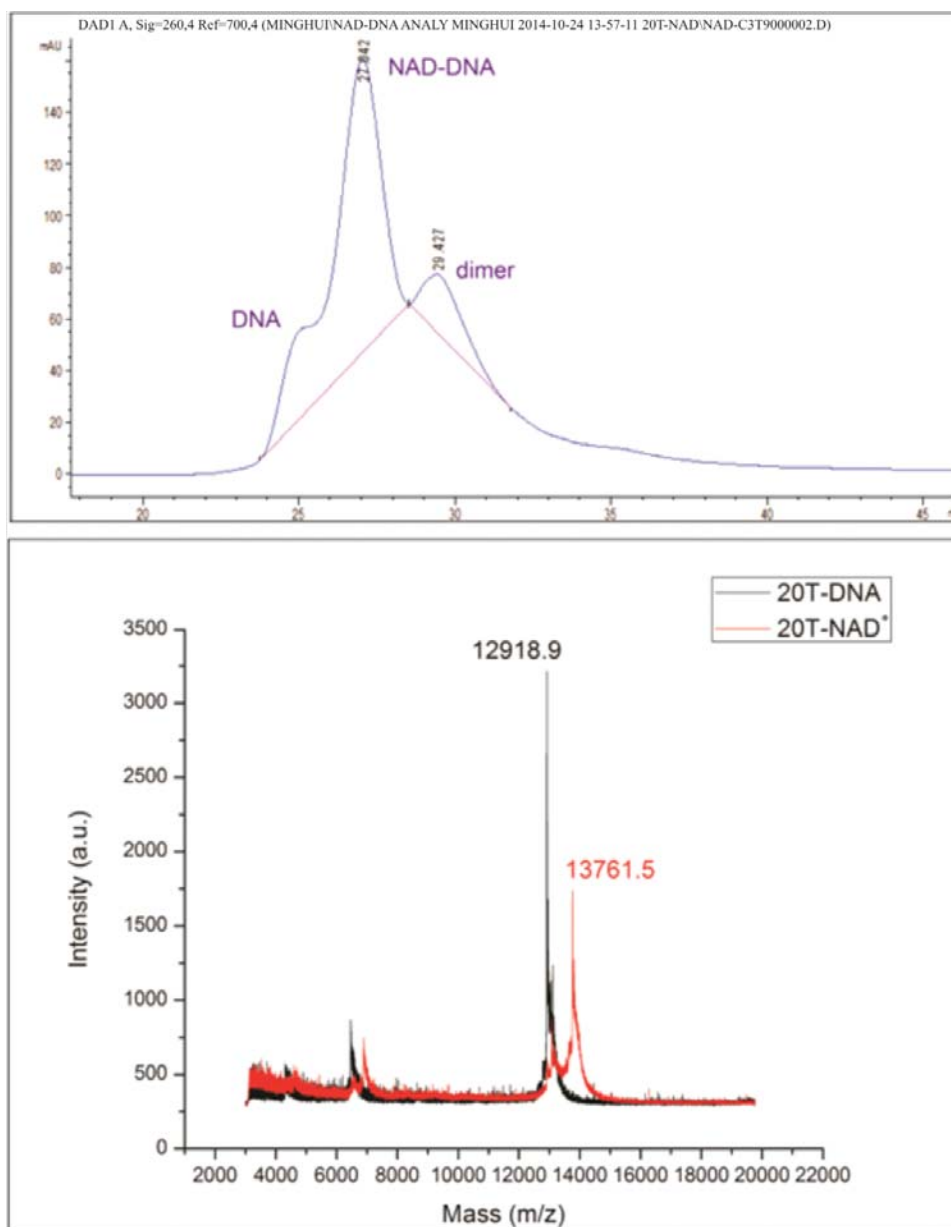


Fig. S2. HPLC purification (top) and MS characterization (bottom) of NAD⁺-modified oligonucleotides (T9-20T) that are designed to be compatible with the 3T3bp, 1T3bp, 1T4bp and 1T5bp tweezers. The calculated molecular weight of T9-20T is 12,927.5 Da (provided by Integrated DNA Technologies, Inc., Coralville, IA, USA). Since the sample concentration was at the scale of nanomolar, it was purified using a C18 analytical column. Due to the overlap of the two peaks in the top panel, we chose the purer portion of each peak with little overlap. Although the purity may not be 100%, the enzyme activities of opened- and closed-state tweezers were compared for the same samples, and therefore the relative activity of the tweezers should not be affected by the conjugation yield and purity of the NAD⁺-DNA conjugates. The peak at ~7000 (m/z) in the bottom panel is a doubly-charged complex.

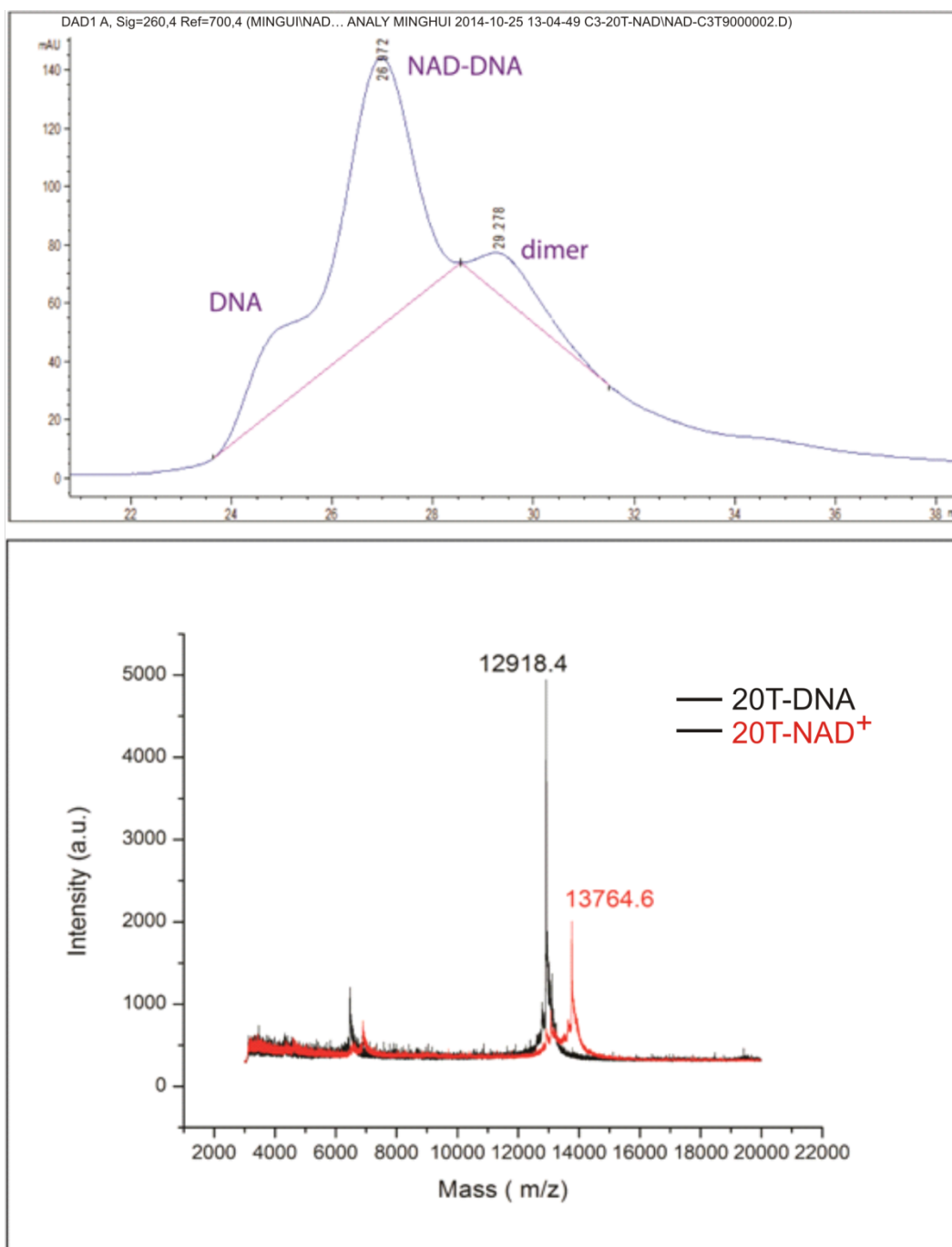


Fig. S3. HPLC purification (top) and MS characterization (bottom) of NAD⁺-modified oligonucleotides (T9-20T) that are designed to be anchored to the 1T4bp-5HJs-iso-I tweezer. The calculated molecular weight of T9-20T is 12,927.5 Da (provided by Integrated DNA Technologies, IDT). Please see legend of Fig. S2 for purification details.

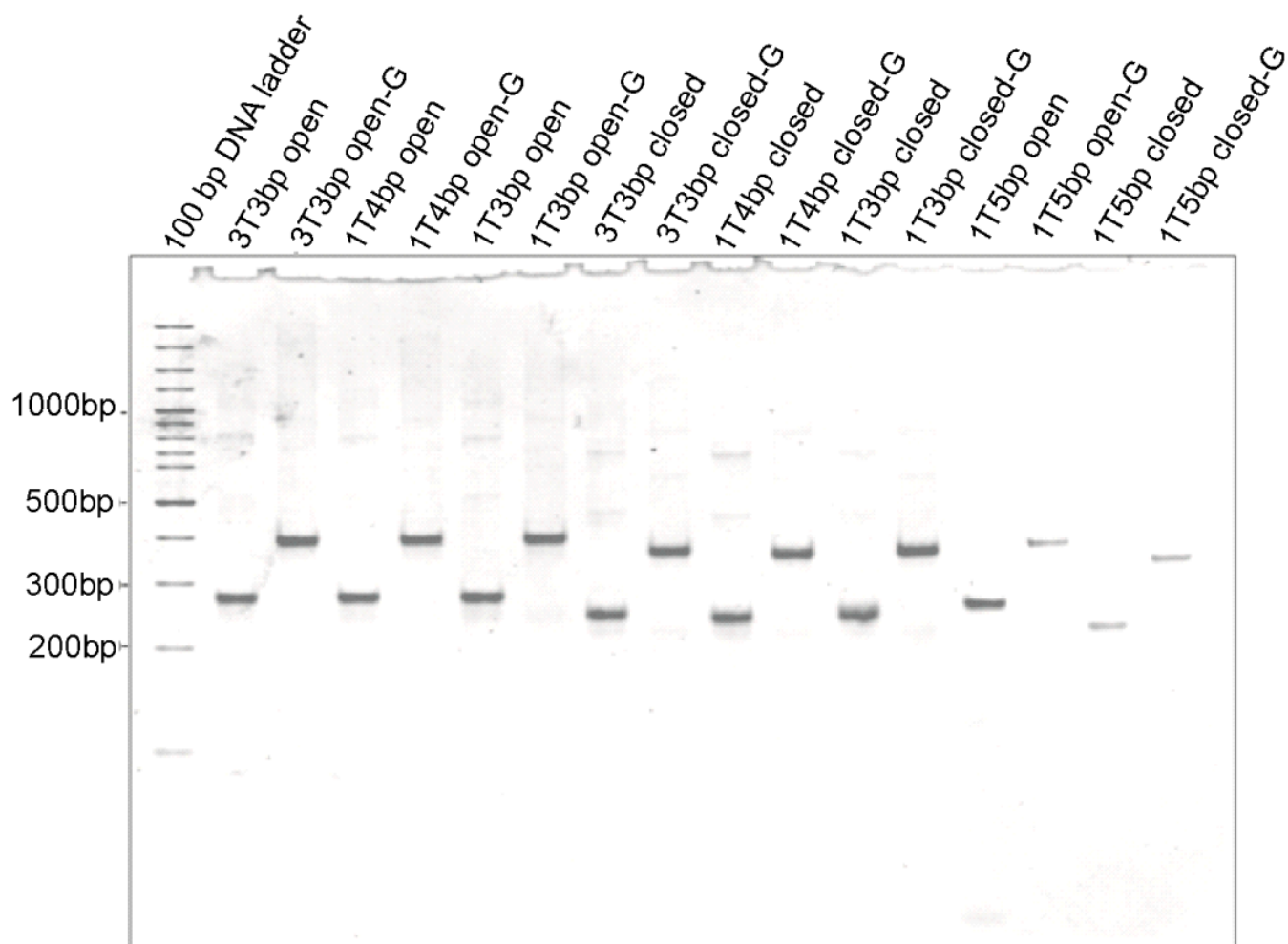


Fig. S4. Native 3% PAGE characterization of the various assembled DNA tweezers used in bulk measurements (summarized in Table S9) with variant actuator elements as indicated. The native polyacrylamide gel was stained with ethidium bromide. Both closed- and opened-state tweezers with 3T/1T-spacers and 3bp/4bp/5bp-stems were analyzed (G: G6pDH enzyme).

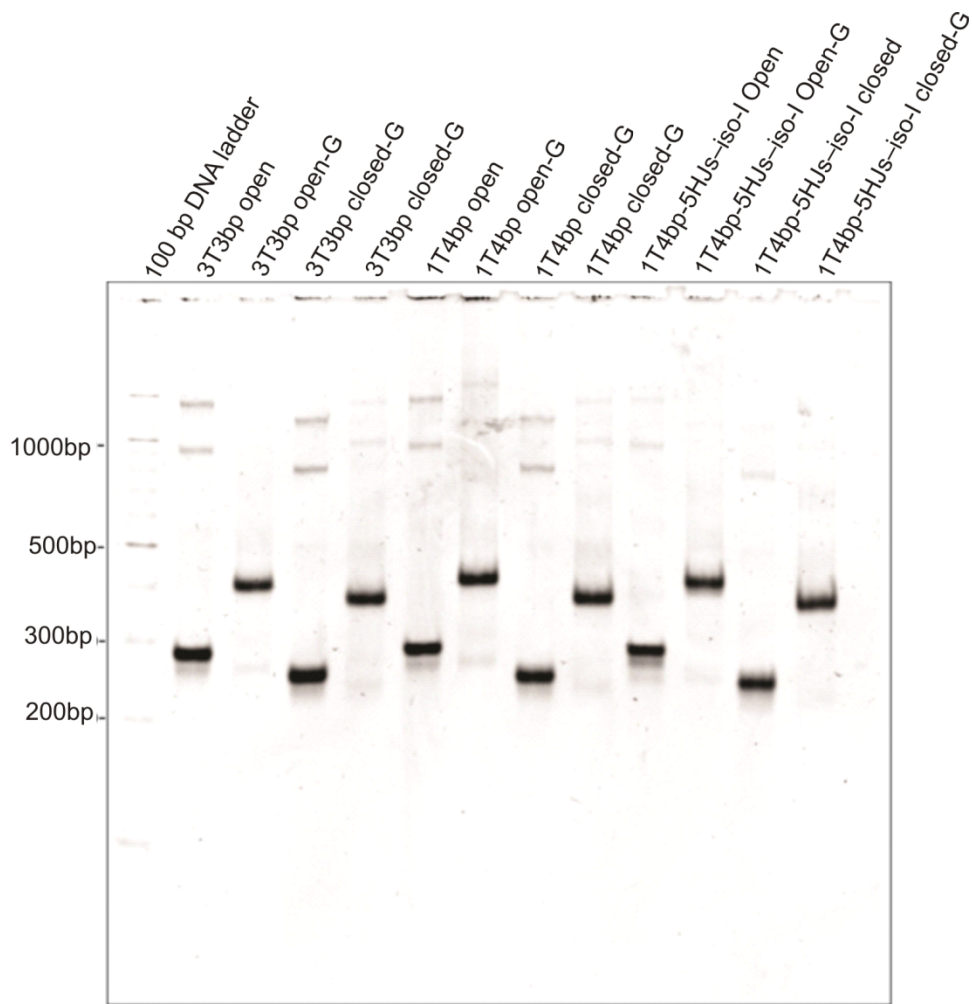


Fig. S5. Native 3% PAGE characterization of the various assembled DNA tweezers used in bulk measurements (shown in Fig. S26) with variant actuator elements as indicated. The native polyacrylamide gel was stained with ethidium bromide. Both closed- and opened-state tweezers were tested (G: G6pDH enzyme).

Section 2: Single molecule FRET (smFRET) characterization of DNA tweezers

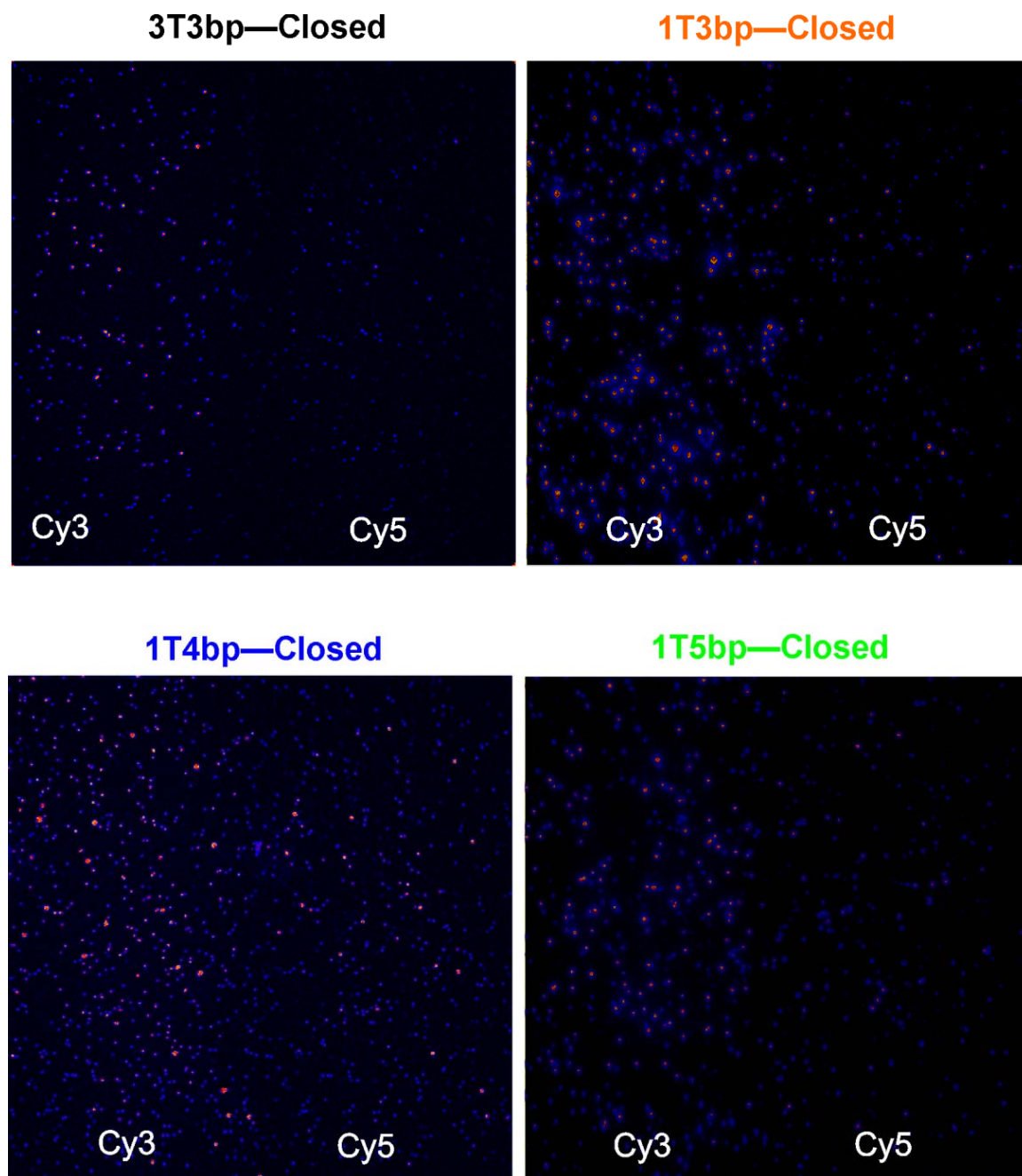


Fig. S6. Representative fields of view of different tweezer designs from single molecule TIRFM observation. The field of view was excited with a green laser (532 nm) and the emission intensity monitored for both the Cy3 and Cy5 channels (as indicated).

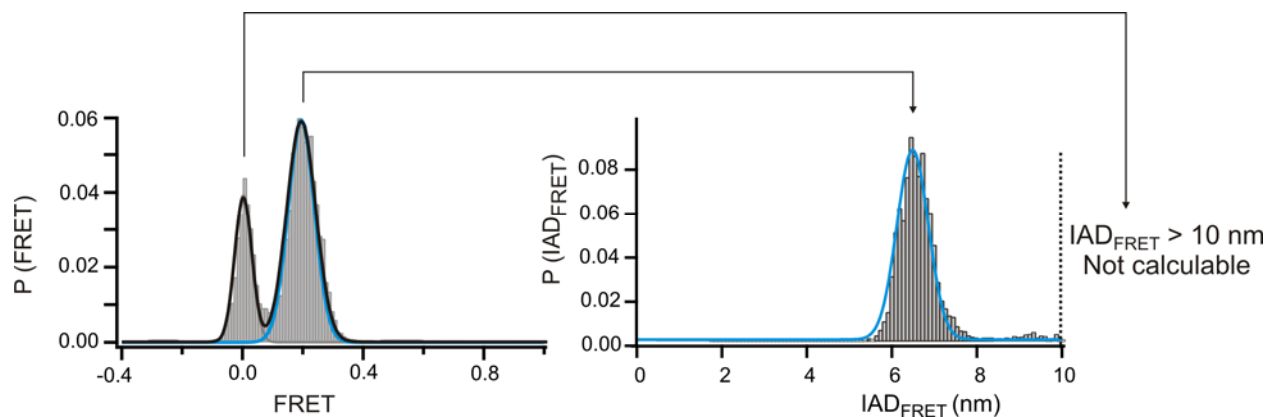


Fig. S7. Determining the IAD_{FRET} of the closed-state 3T3bp tweezer from smFRET data. The FRET data for the right peak (~ 0.2) were first converted into an IAD_{FRET} distribution (as indicated by an arrow) and the mean IAD_{FRET} determined by Gaussian fitting (cyan) of the IAD_{FRET} histogram (right). The zero-FRET population represents a tweezer conformation with an $IAD_{\text{FRET}} > 10$ nm, which cannot be accurately calculated from the data.

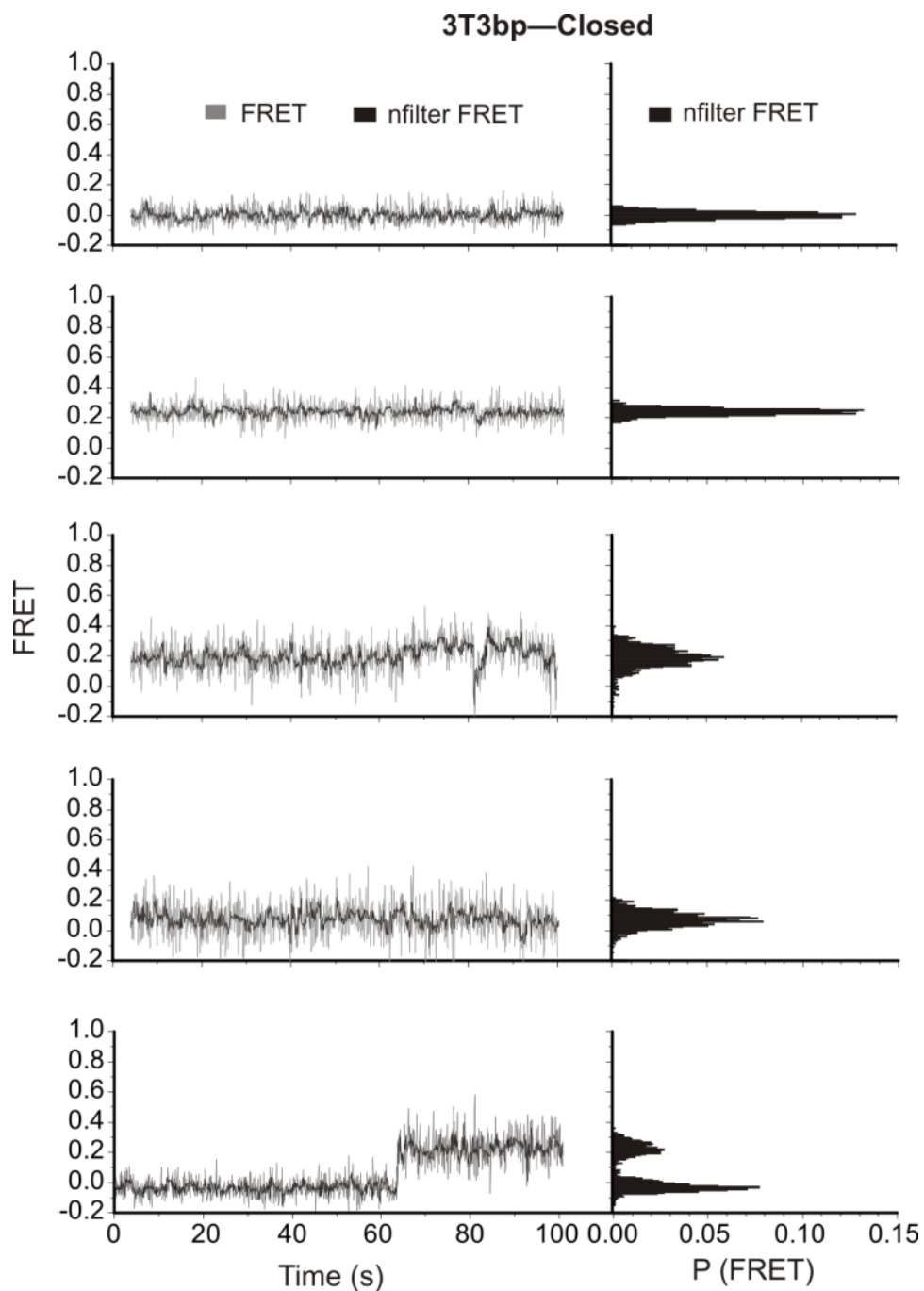


Fig. S8. Representative smFRET traces (gray) of the closed-state 3T3bp tweezer and the corresponding histograms of the nfiltered data (black overlay). A majority of molecules (72%) show static FRET states; although possibly not all underlying sub-states were resolved since the tweezer molecules only span the low FRET regime where the sensitivity to distance changes is low.

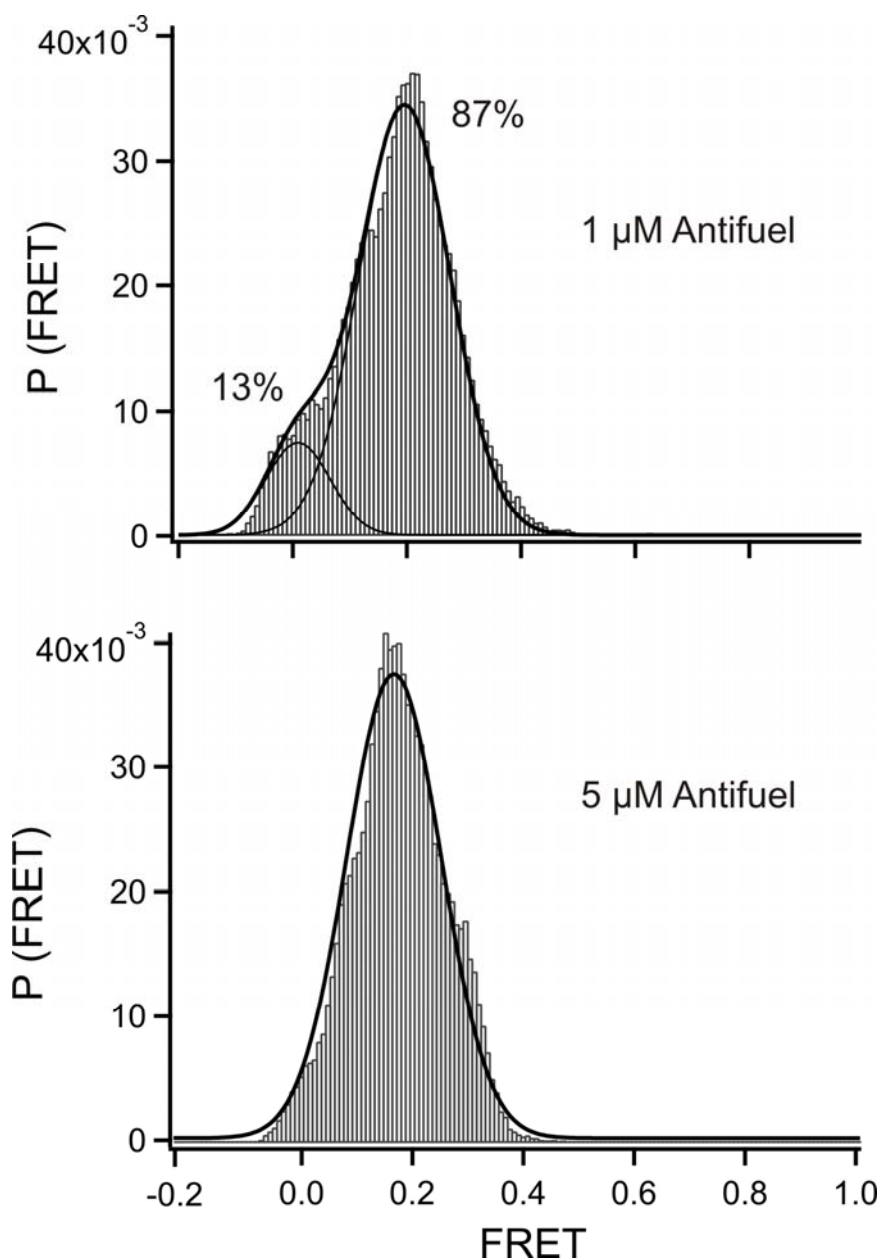


Fig. S9. smFRET probability distributions of the closed-state 3T3bp tweezer at higher concentrations of antifuel strand used to close them. These FRET experiments were conducted in the presence of 1 or 5 μ M antifuel strand in the imaging buffer. Compared to our standard conditions of 0.5-1 μ M antifuel strand during incubation that was later diluted out and led to the data in Fig. 2b (top panel), the zero-FRET population significantly decreased at a 1 μ M antifuel strand concentration and completely disappeared at 5 μ M antifuel strand, strongly suggesting that any zero-FRET state molecules represent unclosed tweezers.

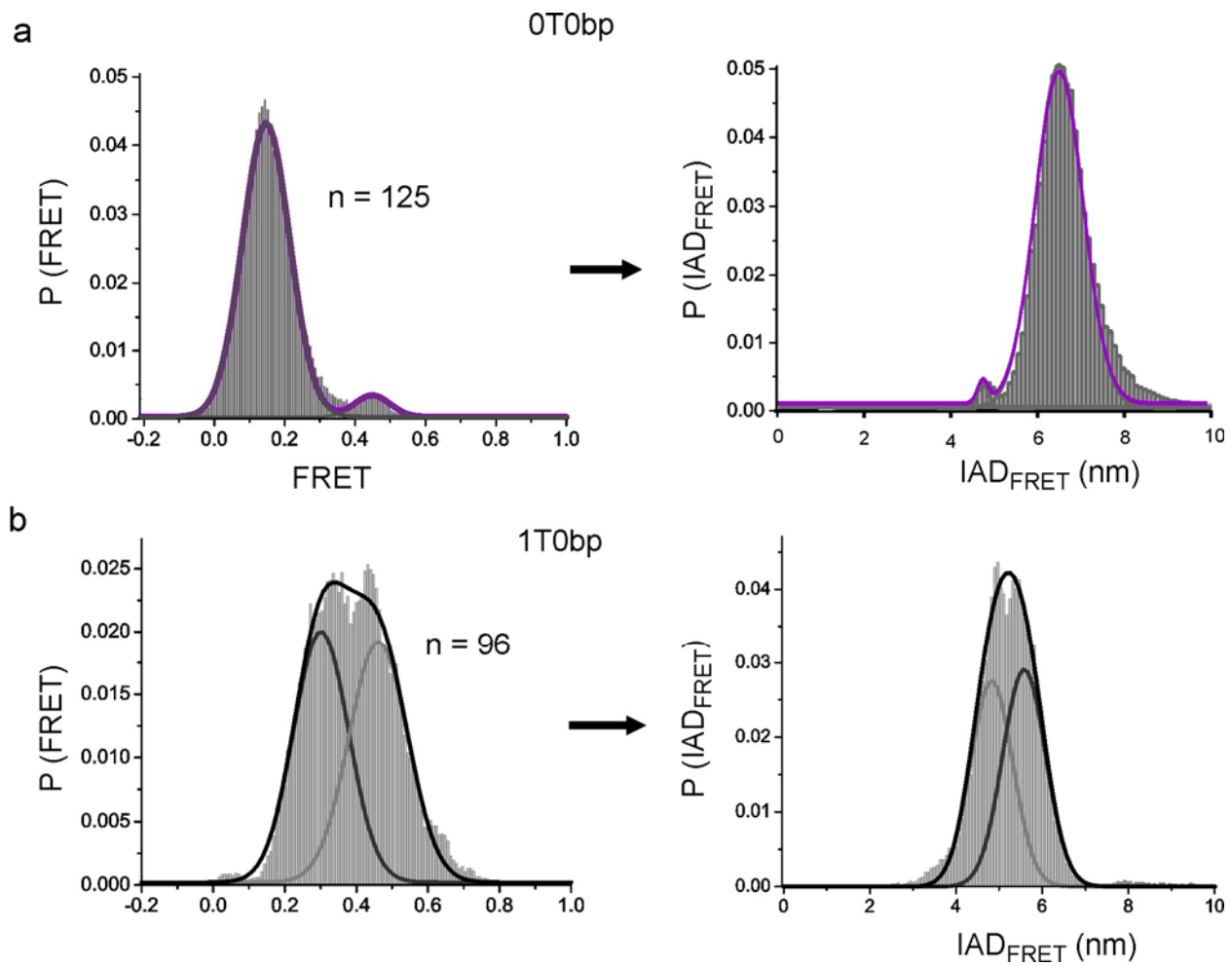


Fig. S10. smFRET probability distribution (left) and corresponding IAD_{FRET} distribution (right) of the OT0bp tweezer (a) and 1T0bp tweezer (b).

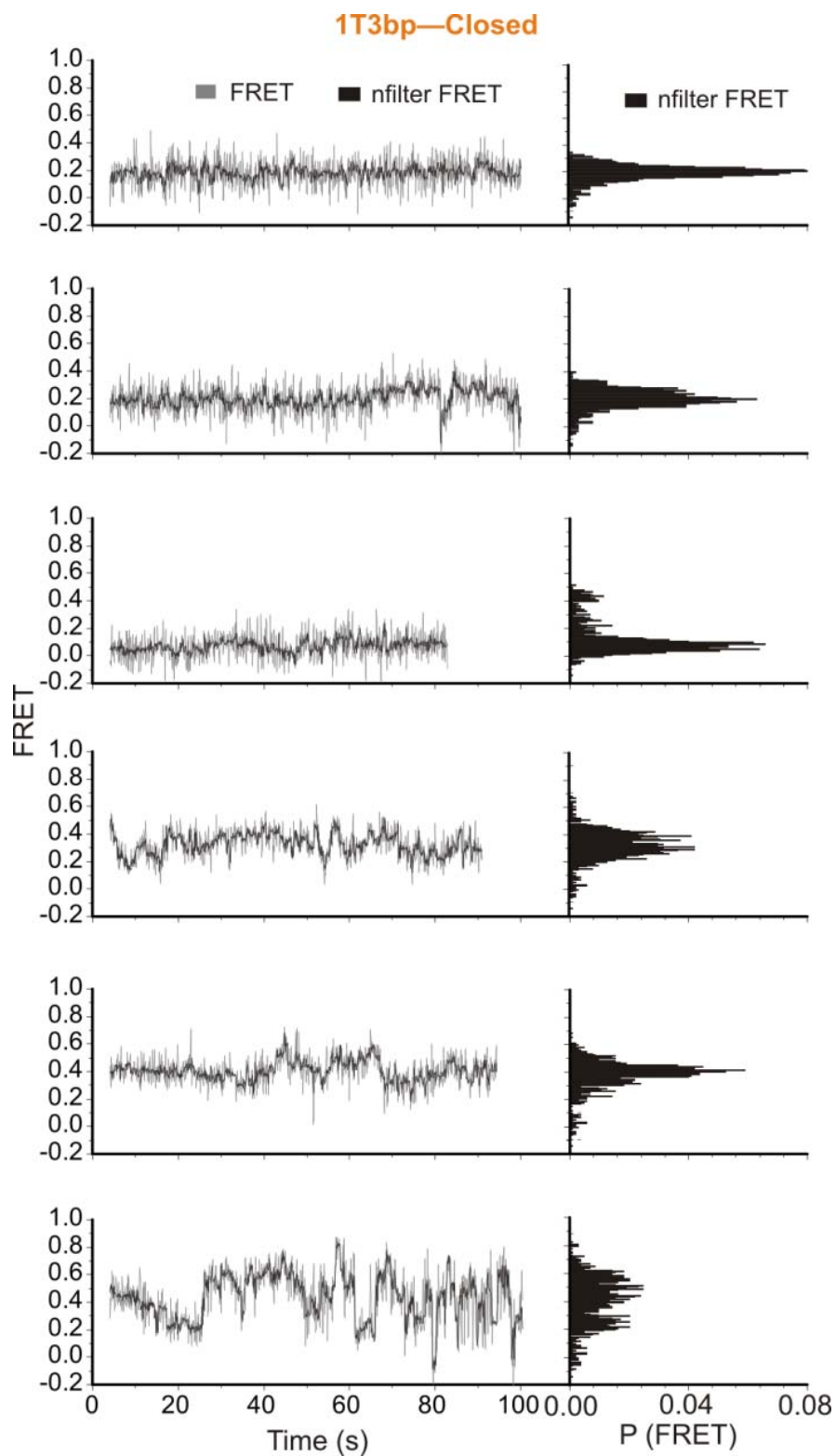


Fig. S11. Representative smFRET traces (gray) of the closed-state 1T3bp tweezer and the corresponding histograms of the nfiltered data (black). A vast majority of the molecules (84%) show dynamic behavior.

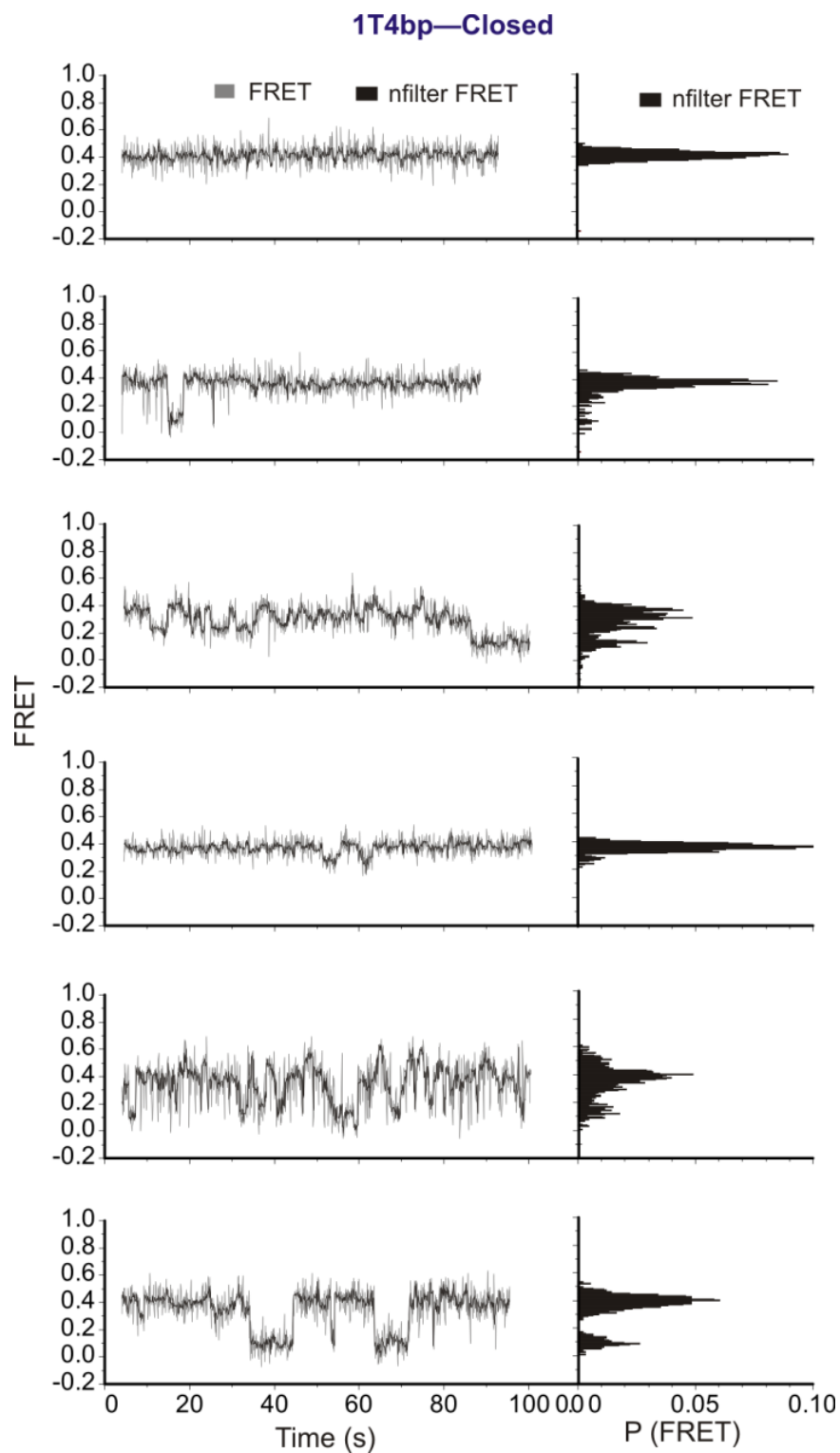


Fig. S12. Representative smFRET traces (gray) of the closed-state 1T4bp tweezer and the corresponding histograms of the nfiltered data (black). A vast majority of the molecules (89%) show dynamic behavior.

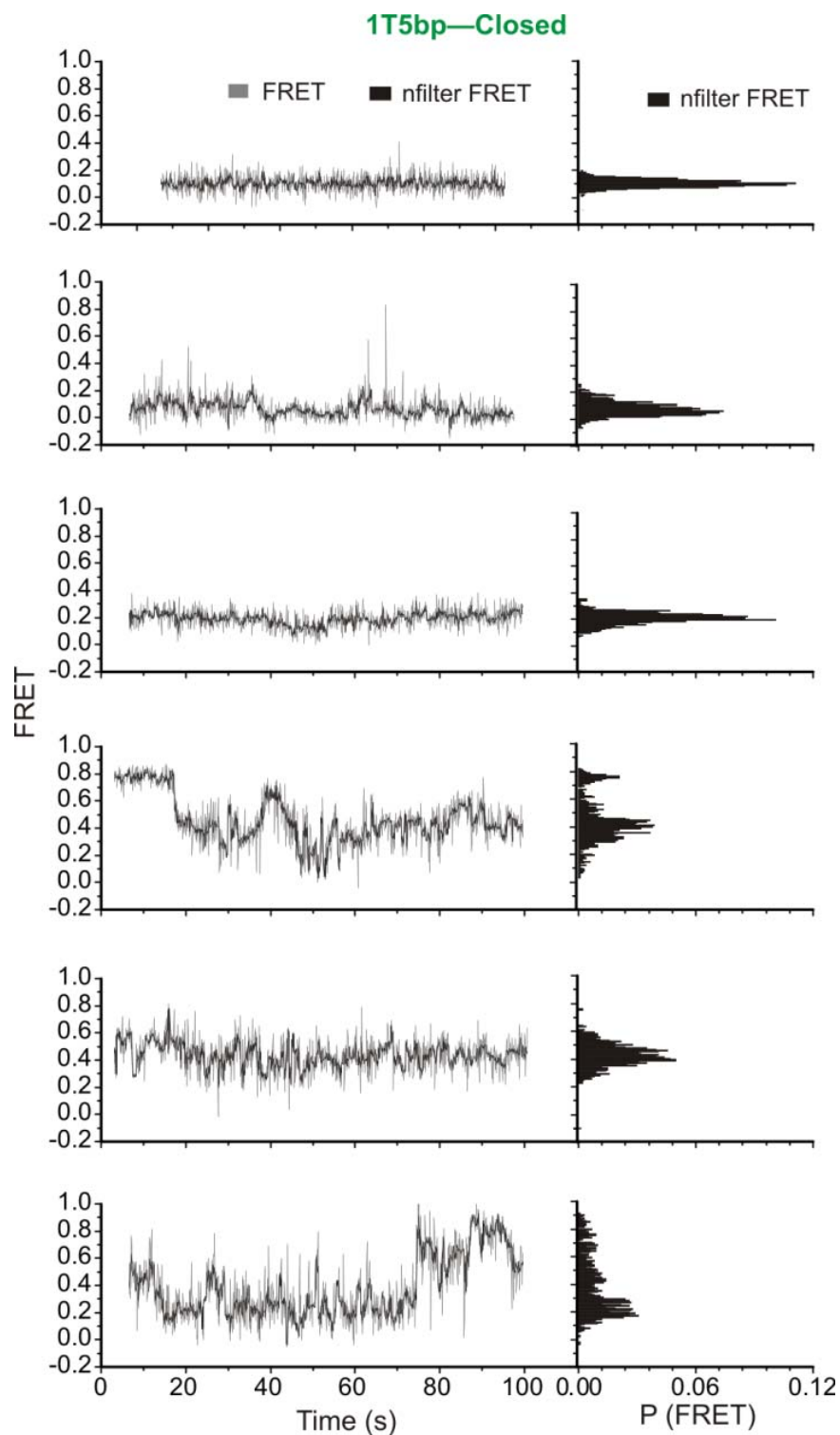


Fig. S13. Representative smFRET traces (gray) of the closed-state 1T5bp tweezer and the corresponding histograms of the nfiltered data (black). A vast majority of the molecules (75%) show dynamic behavior.

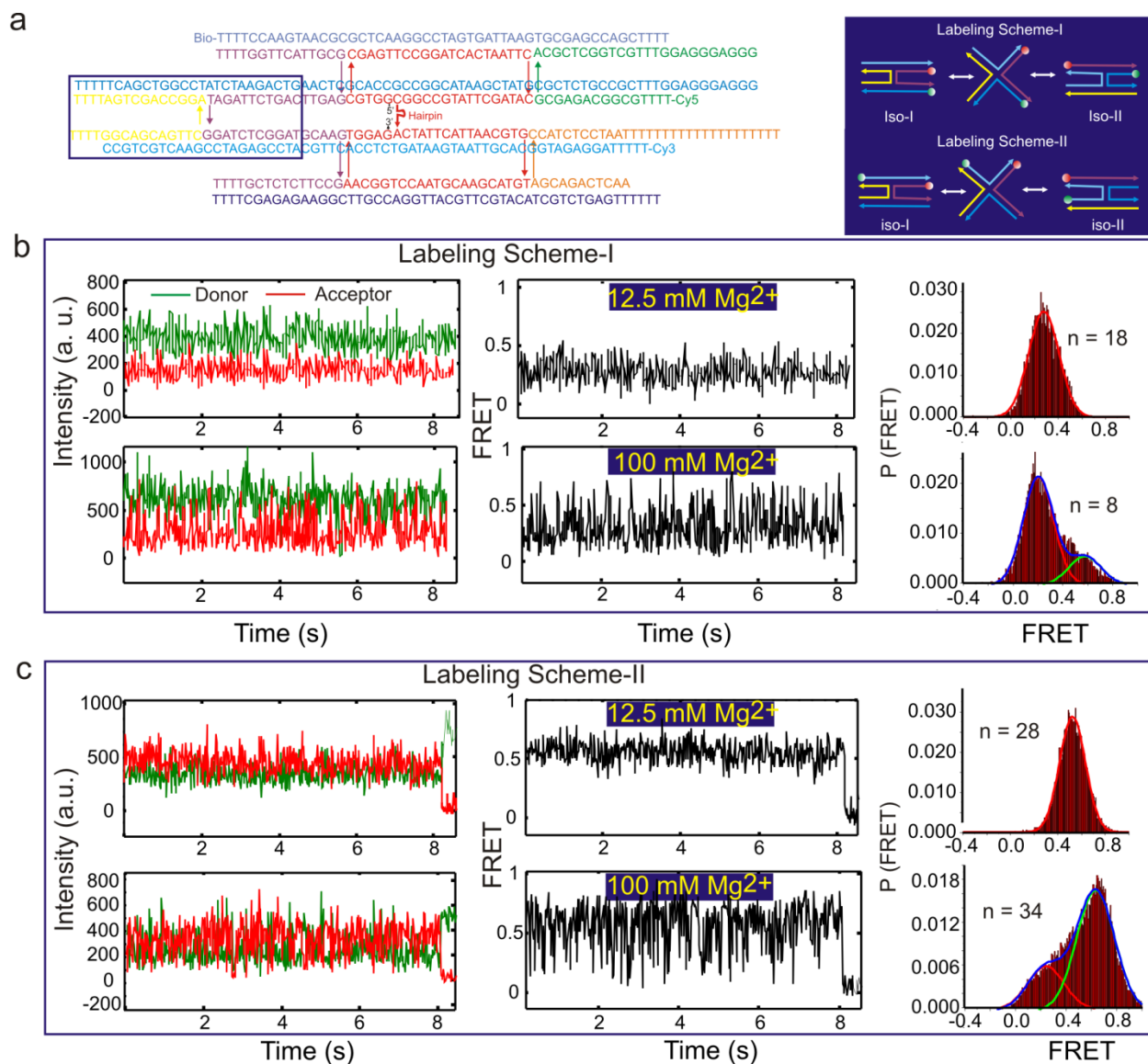


Fig. S14. smFRET measurement of the isolated Holliday Junction (HJ) ‘hinge’ at 16 ms time resolution. The time resolution of 16 ms was achieved by scanning a very small slice (80×512 pixel) at the middle of the chip yielding only few (~ 3 -10) molecules with active FRET pair per field of view. (a) The isolated HJ (blue box, left panel, see Table S5 for detailed sequences) and two complementary labeling schemes (right panel) used in this study. (b) Typical donor (green), acceptor (red), and FRET (black) traces for labeling scheme-I at 12.5 (top panel) and 100 mM Mg²⁺ (bottom panel). The corresponding FRET probability distributions are shown on the right. (c) Typical donor (green), acceptor (red), and FRET (black) traces for labeling scheme-II at 12.5 (top panel) and 100 mM Mg²⁺ (bottom panel). The corresponding FRET probability distributions are shown on the right.

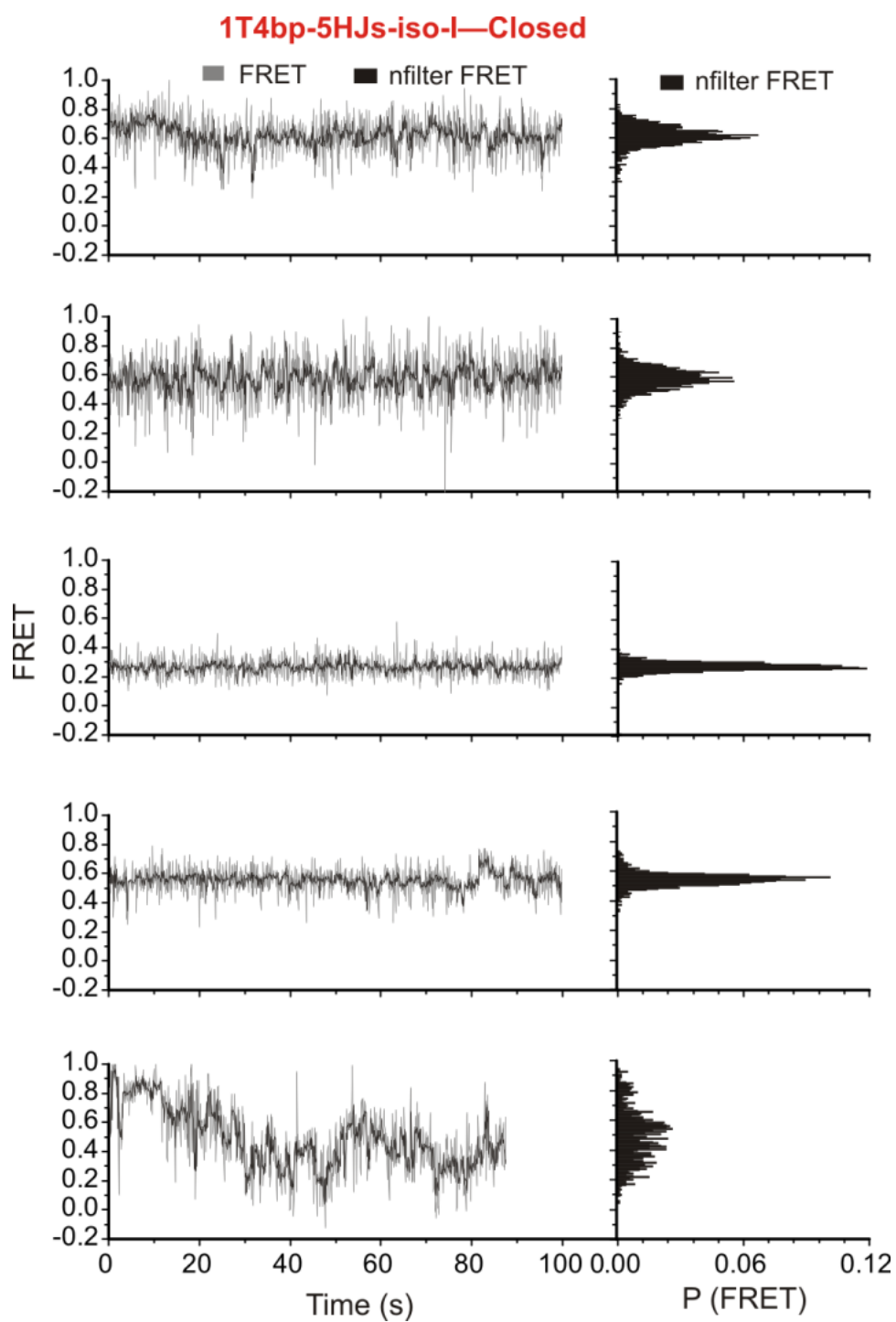


Fig. S15. Representative smFRET traces (gray) of the redesigned closed-state tweezer (1T4bp-5HJs-iso-I) and the corresponding histograms of the nfiltered data (black). Contrary to tweezers with the original HJs, a vast majority of the molecules (90%) in this tweezer show a static (stable) FRET state.

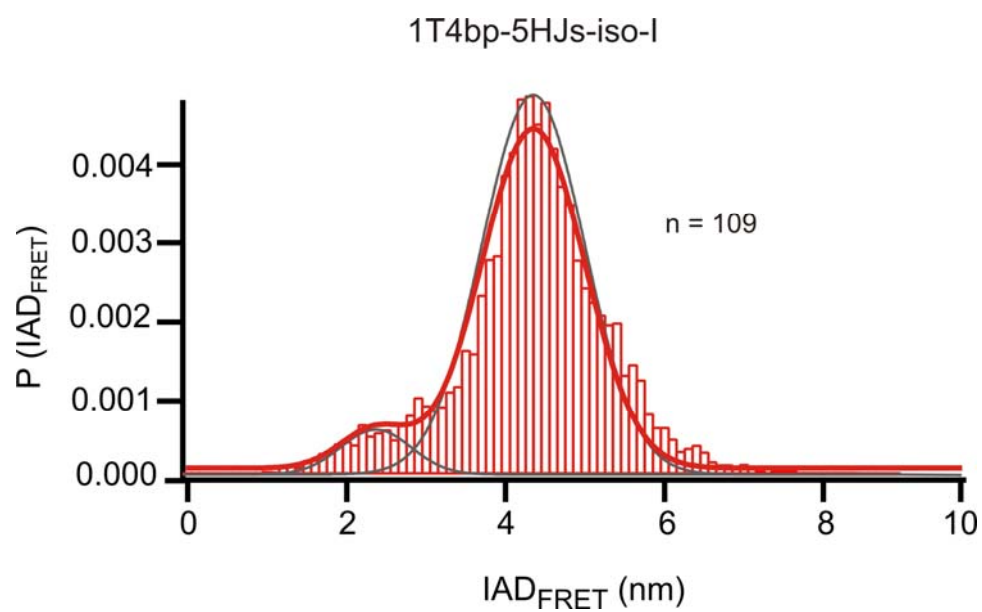


Fig. S16. IAD_{FRET} probability distribution of 1T4bp-5HJs-iso-I tweezers. The number of molecules analyzed is denoted by n .

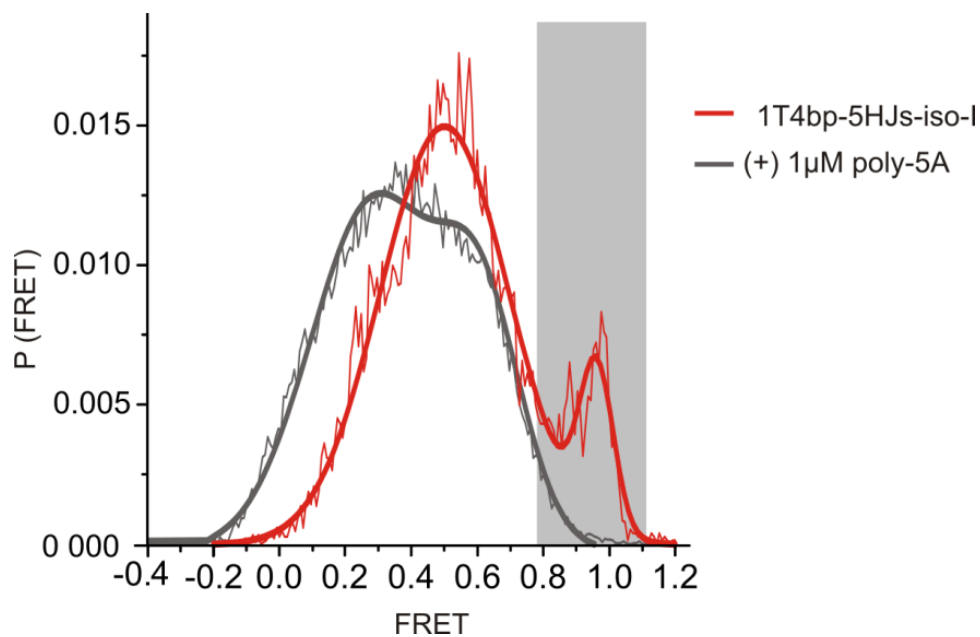


Fig. S17. Comparing the smFRET probability distributions of the 1T4bp-5HJs-iso-I tweezer with and without externally added dA₅ DNA oligonucleotide. The addition of the dA₅ oligonucleotide shifted the probability distribution to lower FRET and the FRET \approx 1.0 population (shaded) disappeared. The FRET probability distribution in the absence of the dA₅ oligonucleotide was taken from Fig. 3a for comparison.

Section 3: Atomic force microscopy (AFM) imaging of DNA tweezers

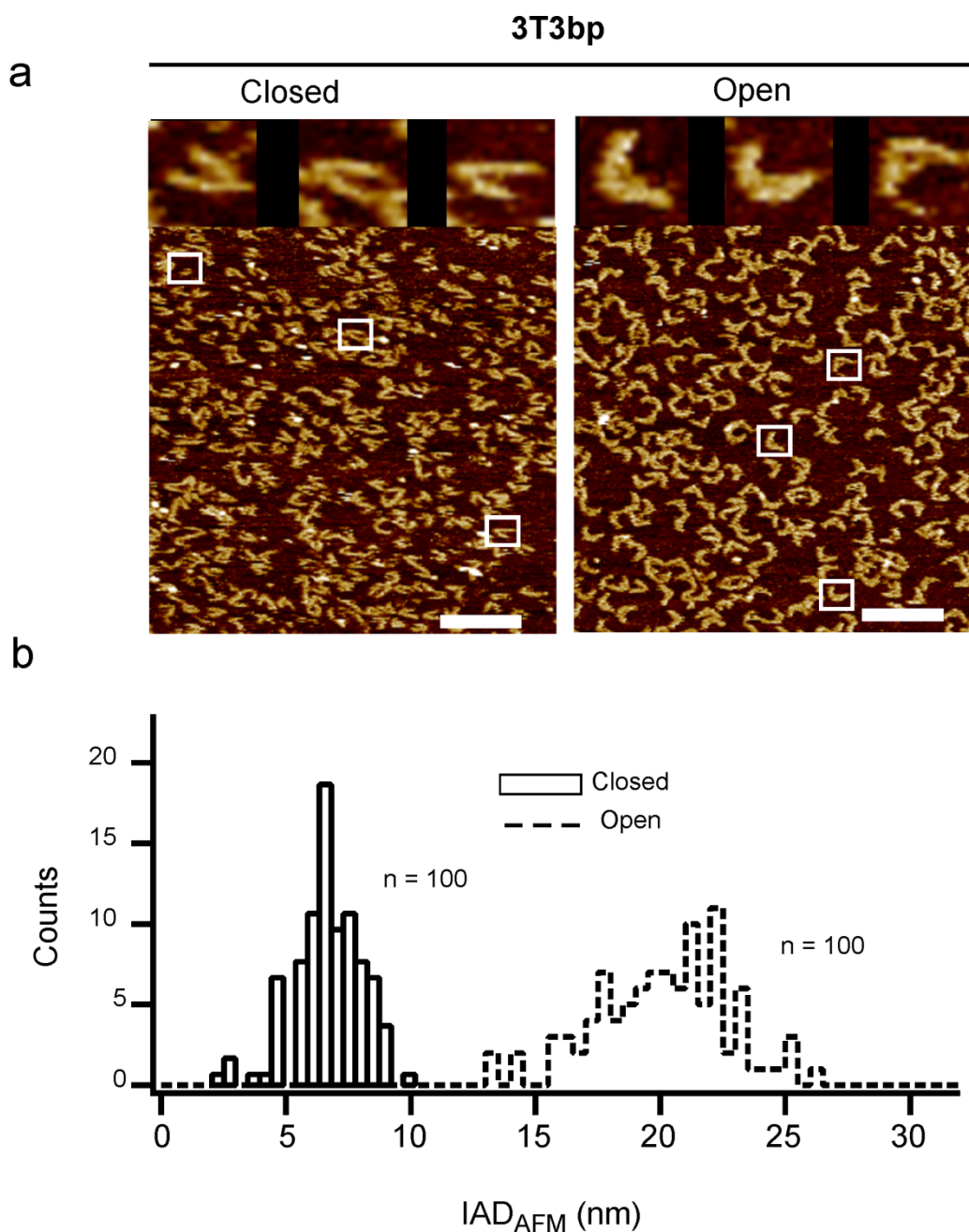
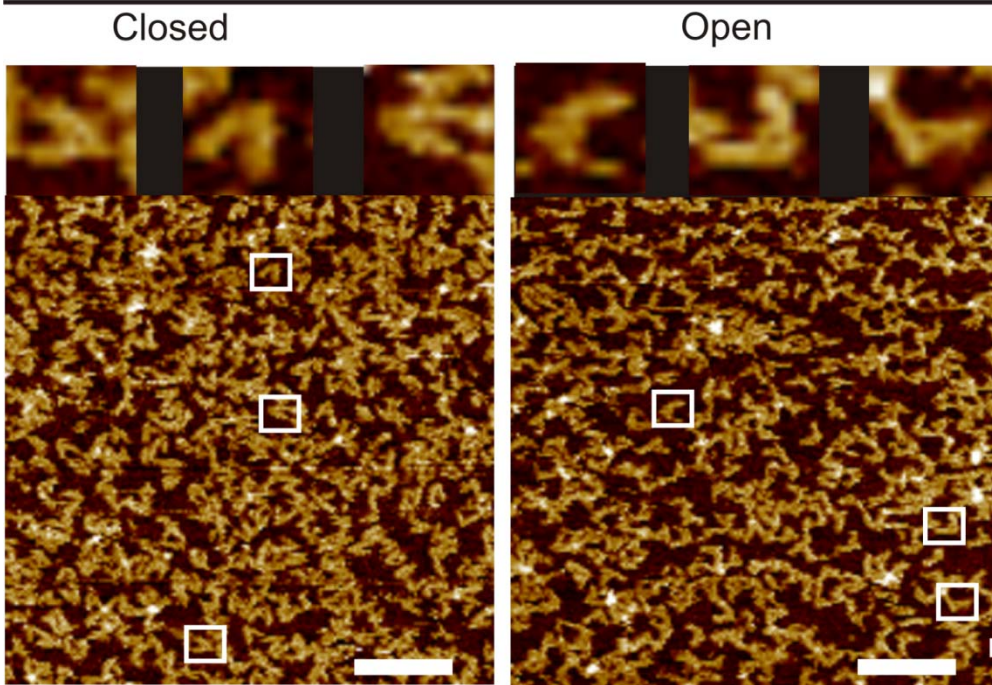
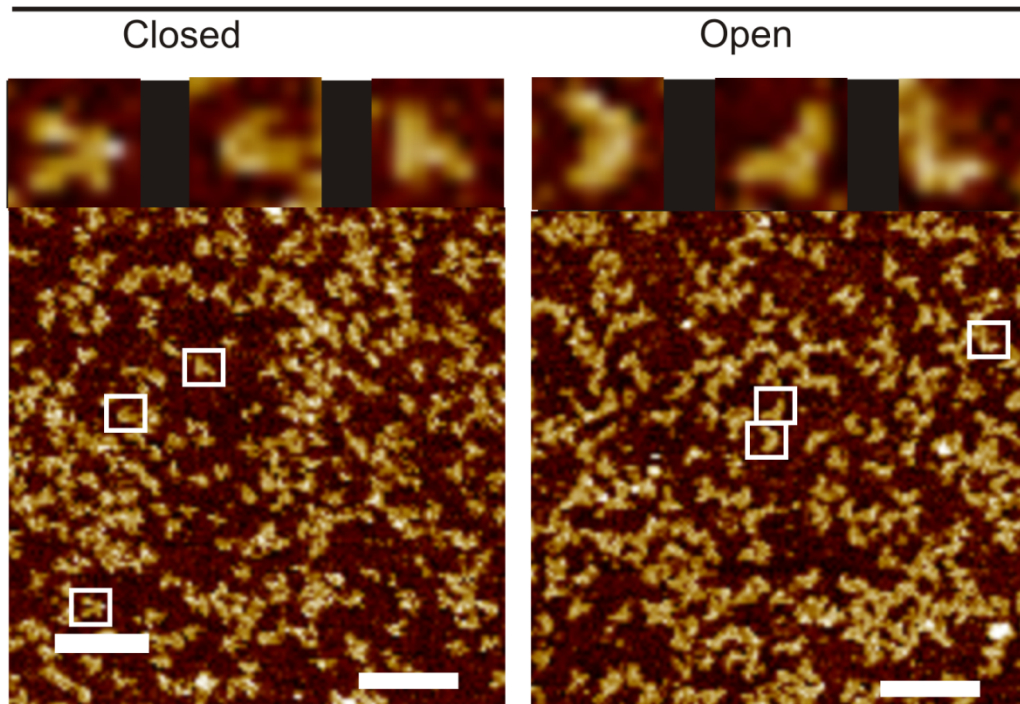


Fig. S18. AFM characterization of the 3T3bp tweezer. (a) Closed- and opened-state tweezers are shown in the left and right panel, respectively. The zoomed-in images of the tweezers ($42 \text{ nm} \times 42 \text{ nm}$) are shown in the same order as they appear (highlighted by boxes) from left to right in the field of view. (b) IAD_{AFM} population distribution for the closed- (black) and opened-state (red) tweezers, where n depicts the number of tweezers analyzed.

1T3bp



1T4bp



Contd....

1T5bp

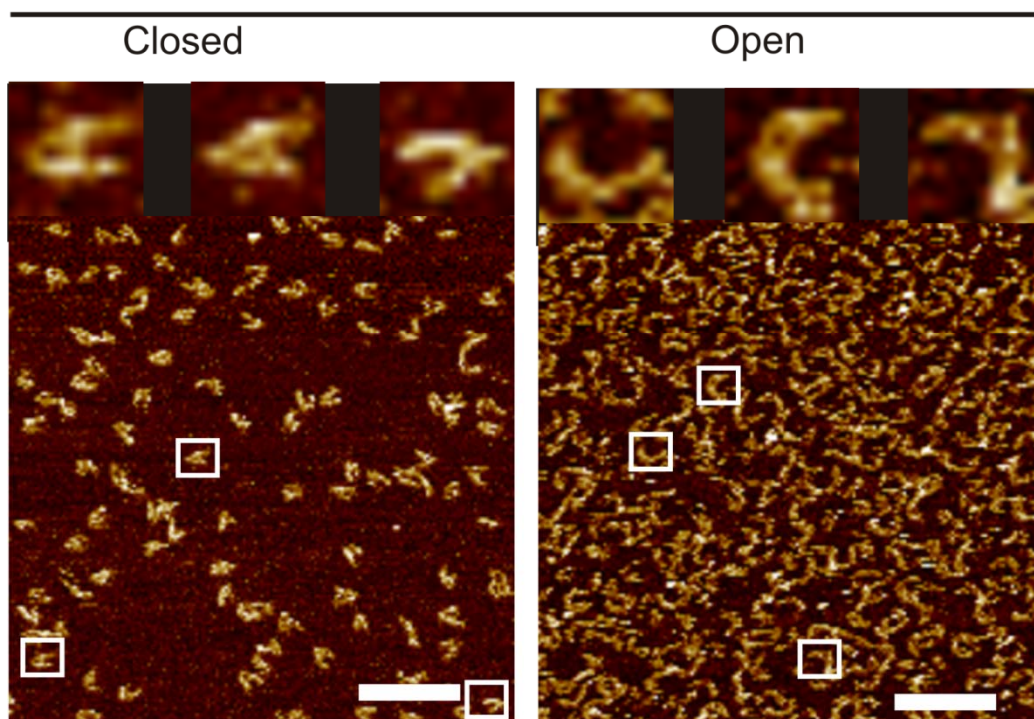


Fig. S19. Expanded field of view of the 1T3bp, 1T4bp and 1T5bp tweezers shown in Fig. 2c. Closed- and opened-state tweezers are shown in the left and right panel, respectively. The zoomed-in images of the tweezers ($42 \text{ nm} \times 42 \text{ nm}$ are shown) are placed in the same order as they (highlighted by boxes) appear from left to right in the field of view.

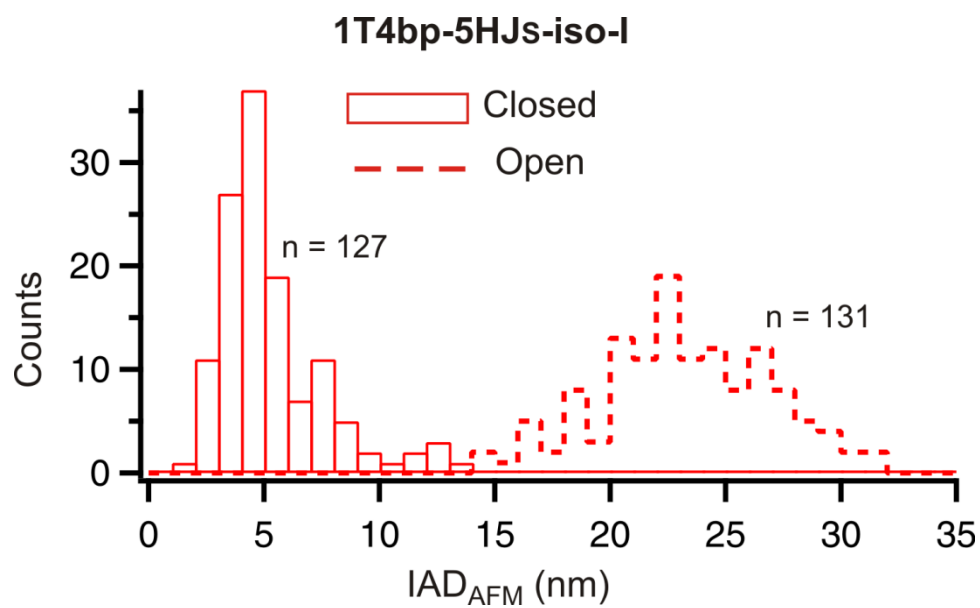


Fig. S20. AFM characterization of the 1T4bp-5HJs-iso-I tweezer. IAD_{AFM} population distribution for the closed- (solid bars) and opened-state (dotted bars) tweezers, where n depicts the number of tweezers analyzed.

Section 4: Molecular dynamics (MD) simulation of DNA tweezers

Table S7: MD simulations reported in this work. Reported are the design of the DNA tweezer^a, the junction sequence^b, where 5HJs-iso-I refers to the case where all five HJs are redesigned to Seeman's junction (J1) in their favored isomer¹⁻³, the inclusion of explicit poly-thymine dye linkers^c, the concentration of magnesium^d, and the duration of each simulation^e. The hairpin was eliminated entirely in the 0T0bp and 1T0bp designs. †While its 3-bp stem is present, the closing loop of the hairpin-actuator was excluded for simplicity in the simulation due to its long equilibration time. Due to its size, and its anticipated slow dynamics, the hairpin would likely contribute to the slowest dynamical modes of the tweezer constructs, i.e., the global bend and twist of the entire structure, and should therefore not affect the inter-arm distance measurements significantly on the reported timescale, provided that the stem remains intact in a given simulation, as confirmed to be the case in the present study.

Tweezer ^a	Junctions ^b	Tails ^c	[Mg ²⁺] ^d	Duration ^e
0T0bp	Original	No	12.5 mM	340 ns
1T0bp	Original	No	12.5 mM	100 ns
1T3bp [†]	Original	No	12.5 mM	100 ns
1T3bp [†]	5HJs-iso-I	No	12.5 mM	100 ns
1T0bp	5HJs-iso-I	Yes	12.5 mM	200 ns
1T3bp [†]	Original	Yes	12.5 mM	200 ns
1T3bp [†]	5HJs-iso-I	Yes	12.5 mM	200 ns
3T3bp [†]	Original	Yes	12.5 mM	300 ns

Construct- specific methods and results

A. MD simulation of the 3T3bp system: The hairpin motif was built using DS Visualizer's Macromolecules Toolkit. A B-form GCG duplex was modified with three thymine bases per strand and then attached to the base-plate model, followed by energy minimization in vacuum using the same parameters detailed in the general MD protocol. Only the hairpin and spacer atoms were allowed to move during this initial minimization. There was no 13-nt hairpin loop present in this simulation.

B. MD simulations of the 0T0bp and 1T0bp systems with original junction sequences: The single crossover construct (0T0bp) was generated using CanDo⁵. The double thymine crossover (1T0bp) construct was generated from the 0T0bp model by adding two thymine bases to the crossover site of the T7 strand using DS Visualizer's Macromolecules Toolkit. Energy minimization was subsequently performed in vacuum using the same parameters as those detailed in the general MD protocol. All atoms except those corresponding to the hairpin and spacer atoms were constrained during this initial minimization. The 0T0bp construct exhibits significant structural out-of-plane distortion (Fig. S21) with a single mean IAD_{MD} of 4.7 nm, whereas the 1T0bp system exhibited two IAD_{MD} sub-populations with mean values of 3.3 nm and 4.3 nm (Fig. 2a and Fig. S22).

D. MD simulations of the 1T3bp system with original and redesigned junction sequences:

In order to elucidate the origin of the distinct states observed using smFRET, we investigated the conformational dynamics of the 1T3bp tweezer (Fig. S24) as a model system in which we excluded the hairpin itself. Justification for this choice is provided by the fact that full equilibration of hairpin conformational dynamics could exceed by orders of magnitude the 100 ns simulations in explicit solvent performed here.⁶ Moreover, because the hairpin itself is likely to remain in solvent due both to solvation energy preference and also entropic considerations, it is unlikely to directly influence the tweezer conformation on the time-scales simulated.

Results of MD simulation indicate that the hairpin stem remains hybridized on the approximately 200 ns timescale simulated (Table S8). Moreover, the duplex stem does not interdigitate between the tweezer's arms on this timescale, consistent with the discussion above. Importantly, the inclusion of explicit thymine dye linker tails had a noticeable effect on the IAD_{MD} due to their non-specific interactions involving hydrogen bonding and partial base pairing and stacking, resulting in two sub-populations centered at 2.7 nm and 3.6 nm respectively (Fig. 3c). Simulation of the same construct excluding these tails resulted in IAD_{MD} sub-populations with mean values of 3.6 nm and 4.3 nm (Fig. 3c), supporting the hypothesis that interactions involving these linkers might stabilize conformational sub-states observed experimentally (Fig. S24a and b). MD shows them to be stabilized by short-lived, non-specific hydrogen bonding interactions between the poly-thymine linkers tethering the dyes to the tweezer arms (Fig. 24b, top panel). However, out-of-plane distortions of the tweezer arms result due to twisting that is incurred by the square lattice.⁷ In contrast to this minimal inter-tail interaction (Fig. S24b, top), the interaction was more prevalent for the same construct with redesigned junctions (Fig. S23 and S24b, bottom panel). For the 1T3bp system with redesigned junction sequences, the effect of including explicit tails significantly reduced IAD_{MD} values when compared with a complementary simulation that does not include the tails (Fig. 3c). Visual inspection of the redesigned structure reveals a more planar conformation (Fig. S23), with significant stabilization of the lower (1.1 nm) distance sub-population by inter-tail interactions (Fig. S24b).

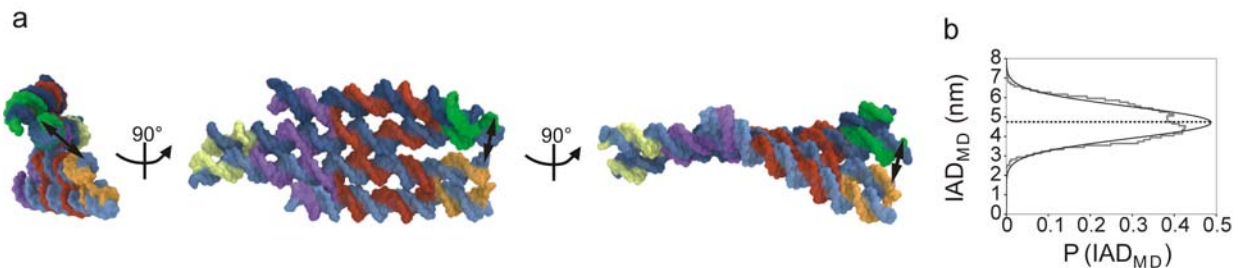


Fig. S21. Three-dimensional configuration of the 0T0bp DNA tweezer. (a) Three orthogonal views of a representative conformation of the tweezer corresponding to mean IAD_{MD} of 4.7 nm. (b) The distribution of IAD_{MD} values from MD simulation and the fitted single Gaussian population, with μ_{0T0bp} of 4.7 nm, is shown.

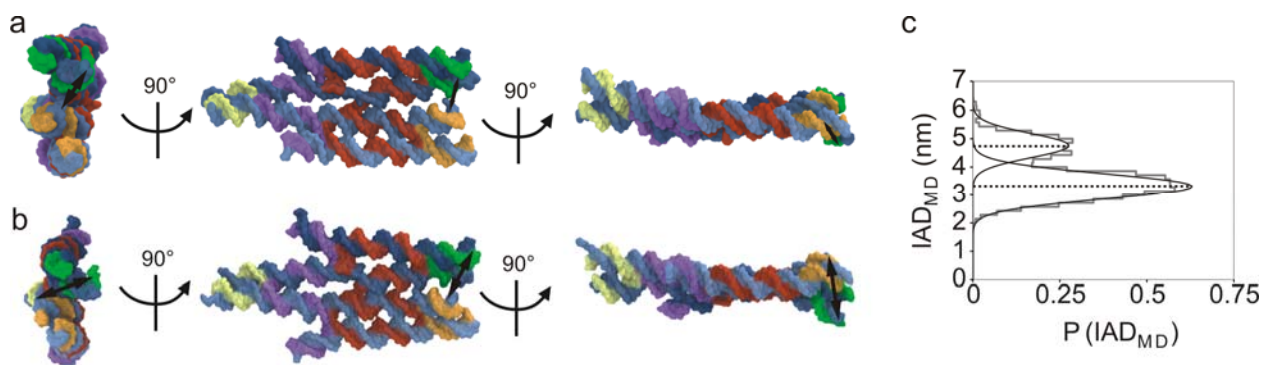


Fig. S22. Three-dimensional configurations of the 1T0bp DNA tweezer. Three orthogonal views of a representative conformation of the tweezer corresponding to mean IAD_{MD} values of (a) 3.3 nm and (b) 4.7 nm. (c) The distributions of IAD_{MD} values from MD simulation and the fitted Gaussian populations.

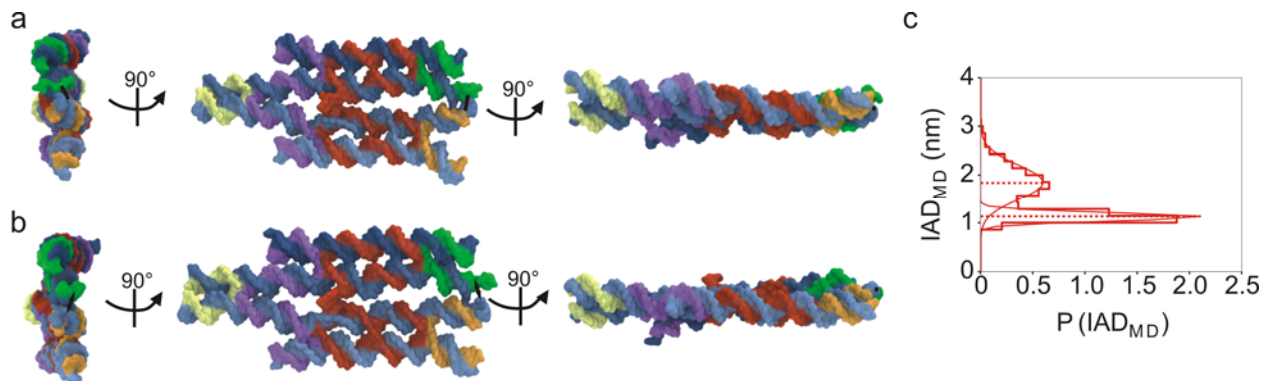


Fig. S23. Three-dimensional configurations of the 1T3bp-5HJs-iso-I DNA tweezer. Three orthogonal views of a representative conformation of the tweezer corresponding to mean IAD_{MD} values of (a) 1.1 nm and (b) 1.8 nm. (c) The distributions of IAD_{MD} values from MD simulation and the fitted Gaussian populations.

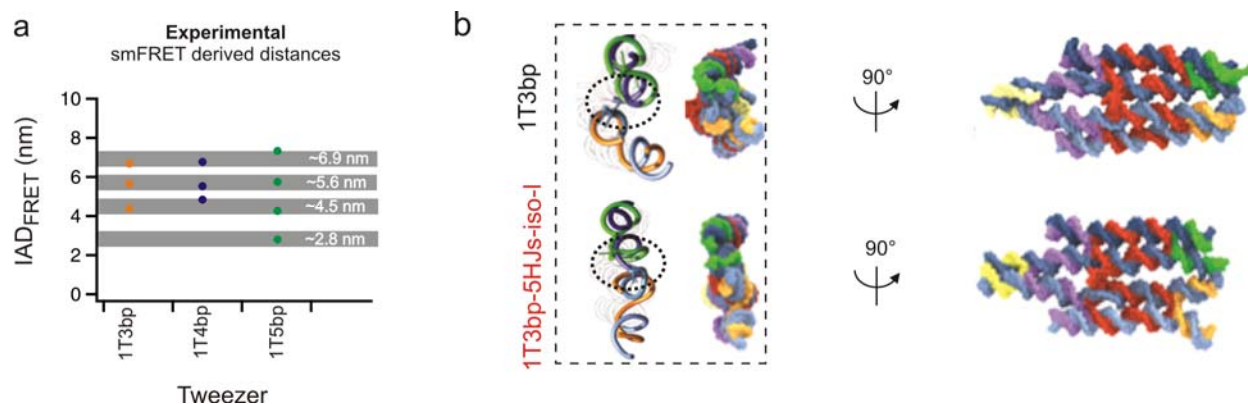


Fig. S24. MD simulation of the 1T3bp tweezer. (a) smFRET derived IADs (IAD_{FRET}) for the non-zero FRET populations in 1T3bp, 1T4bp and 1T5bp tweezers. The shaded areas highlight the common sub-states with nearly the same IAD_{FRET} . (b) Two typical orthogonal views from MD simulation of the 1T3bp construct (top) and junction redesigned 1T3bp-5HJs-iso-I (bottom) tweezers, corresponding to their mean low IAD_{MD} . The tweezer adopted a flatter conformation after redesigning the junctions (dotted box); allowing more prevalent inter-tail interaction (highlighted with dotted circles on the rendered views on the left). This observation was consistent with the conclusion that cooperativity exists between structural flattening and the inter-tail interaction.

MD Movies:

Movie SM1. Movie of the 300 ns MD trajectory for the 3T3bp construct with explicit tails at 300 K and 12.5 mM Mg^{2+} sampled at 7 ns per frame.

Movie SM2. Movie of the 330 ns MD trajectory for the 0T0bp construct without explicit tails at 300 K and 12.5 mM Mg^{2+} sampled at 7 ns per frame.

Movie SM3. Movie of the 100 ns MD trajectory for the 1T0bp construct without explicit tails at 300 K and 12.5 mM Mg^{2+} sampled at 5 ns per frame.

Movie SM4. Movie of the 200 ns MD trajectory for the 1T3bp construct with explicit tails at 300 K and 12.5 mM Mg^{2+} sampled at 7 ns per frame.

Movie SM5. Movie of the 200 ns MD trajectory for the 1T3bp-5HJs-iso-I construct with explicit tails at 300 K and 12.5 mM Mg^{2+} sampled at 7 ns per frame.

Monitoring hairpin stem integrity:

A. Methods: To ensure that the hairpin stem motif remained intact over the course of the simulations, the number of hydrogen bonds present in the short duplex was monitored at each trajectory step for all 1T3bp

systems. The calculations were performed using the MDAnalysis toolkit,⁸ with a donor-acceptor distance of 3.0 Å and an angle cutoff of 120°.

B. Supporting results: All stem motifs remained intact over the course of the production runs for the 1T3bp systems, with the tail-free constructs exhibiting a lower mean number of hydrogen bonds in the stem than their explicit tail counterparts (Table S8). The observation that the tweezer arms are closer in the explicit tail simulations implies that there is probably less tension on the hairpin stem, resulting in a higher number of stable hydrogen bonds.

Table S8: Mean number of hydrogen bonds in stem during production runs.

1T3bp Tweezer	Tails	Mean Hydrogen Bonds In Hairpin Stem
Original Sequence	No	3
Original Sequence	Yes	5
5HJs-iso-I	No	2
5HJs-iso-I	Yes	7

Calculation of base pair structural parameters: The inter-bp structural step parameters were calculated using 3DNA^{9,10} via the *x3DNA* interface within the MDAnalysis toolkit for every simulated structure. Parameter values were calculated for each point of the minimization and equilibration trajectories to ensure that a correct initial structure was being used for production runs.

Section 5: Bulk measurement of tweezer-scaffolded G6pDH activity

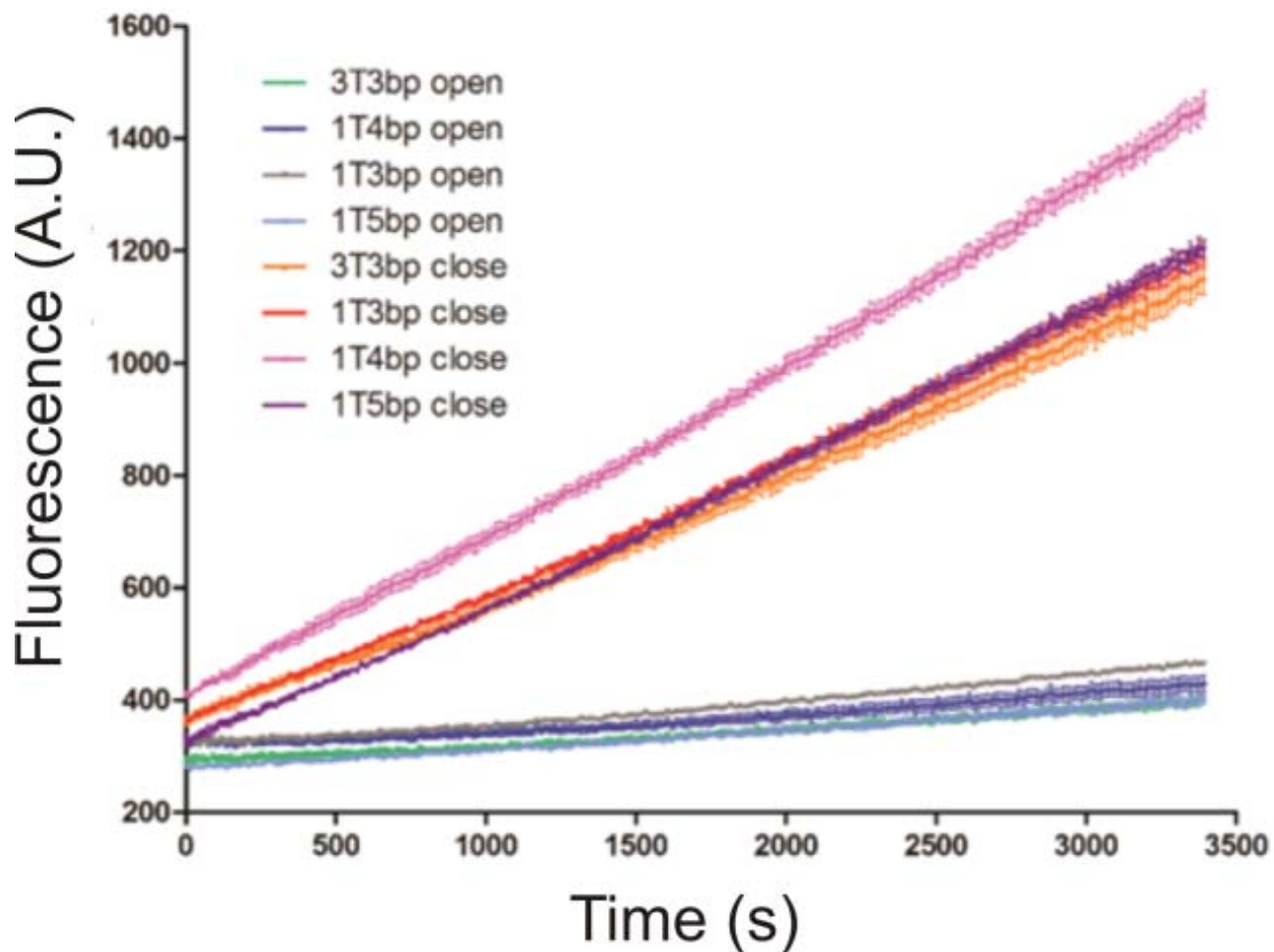


Fig. S25. Raw activity data of opened- and closed-state tweezers with the G6pDH/NAD⁺ pair. Assay conditions: 100 nM G6pDH-NAD⁺ assembly, 1 mM G6p/PMS, 500 μ M resazurin in 1 \times TBS buffer (pH 7.5). A corresponding native gel characterization of the tweezers is shown in Fig. S4. The relative fold enhancement is summarized in Table S9.

Table S9. Bulk measurements of enzyme activity of opened- and closed-state tweezers with the G6pDH/NAD⁺ pair. The relative fold enhancement in activity from opened- to closed-state was calculated by taking the ratio of the activity in closed tweezer (Activity—Closed) to open tweezer (Activity—Open). *1T4bp tweezer demonstrates the highest fold enhancement.

Tweezers	Activity—Open	Activity—Closed	Fold Enhancement \pmSD ($n=3$)
3T3bp	0.060	0.300	5.0 \pm 1.0
1T3bp	0.048	0.257	5.4 \pm 0.2
1T4bp	0.031	0.277	8.8 \pm 0.3*
1T5bp	0.036	0.270	7.5 \pm 0.2

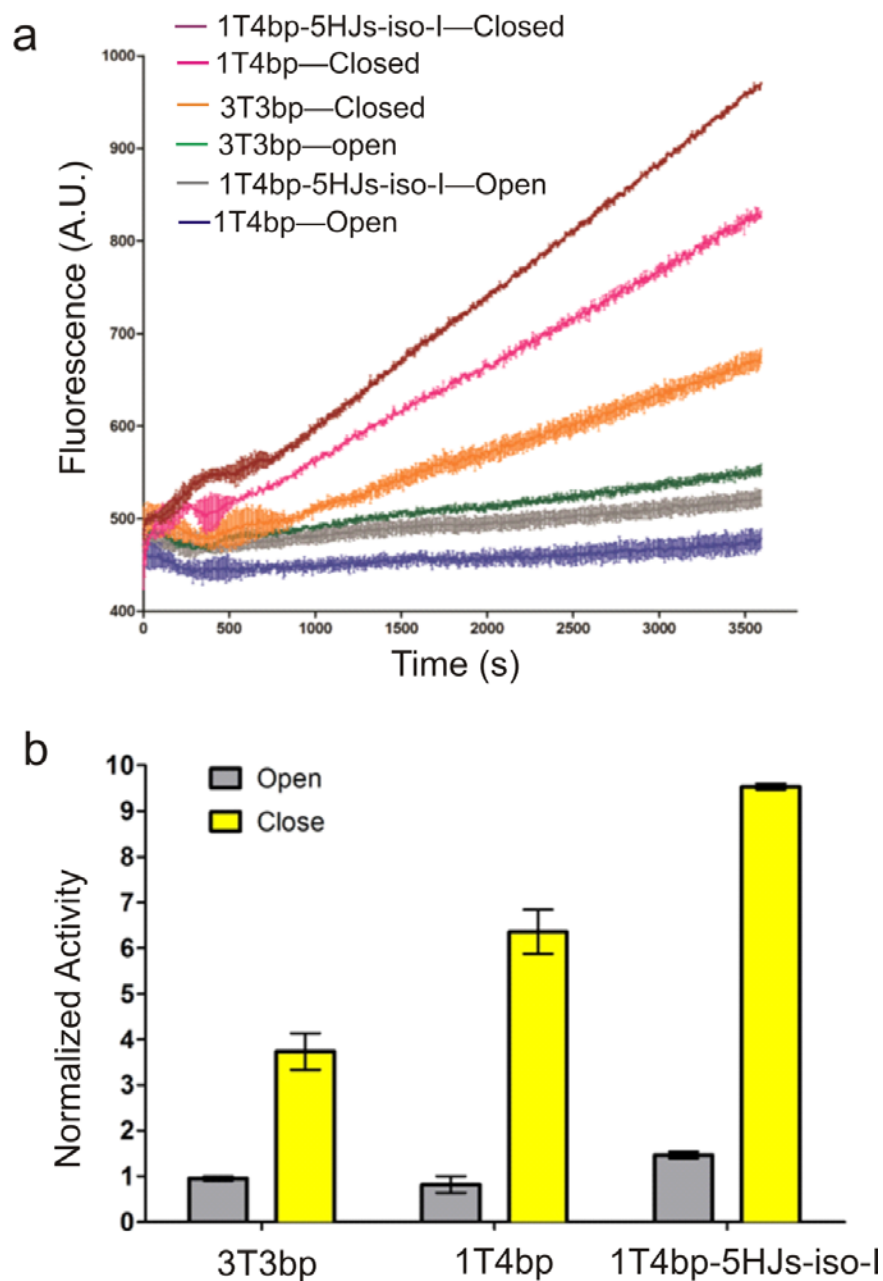


Fig. S26. Bulk measurements of enzyme activity of three design-specific tweezers. Raw data (a) and normalized activity (b) of open and closed 3T3bp/ 1T4bp/ 1T4bp-5HJs-iso-I tweezers with the G6pDH/ NAD⁺ pairs. Activity is normalized with respect to original 3T3bp open tweezers. The disturbance in the fluorescent signal in (a) during the first 500 s may be due to instability of the SoftMax plate reader after inserting the sample plate. This region was excluded for calculating the initial velocity. Assay conditions: 100 nM G6pDH-NAD⁺ assembly, 1 mM G6p/PMS, 500 μ M resazurin in 1 \times TBS buffer (pH 7.5). The corresponding native gel characterization of the tweezers is shown in Fig. S5.

Section 6: Single molecule measurement of tweezer-scaffolded G6pDH activity

Table S10. Reagents used for the single molecule enzyme assay of enzyme/cofactor coupled tweezers. *The concentration of resazurin was optimized to maintain a tolerable background for a reliable TIRFM measurement of enzyme turnover.

Solution	Concentration
10× TBS, pH 7.5	1×
Resazurin	50 nM*
Glucose-6-phosphate (G6p)	1 mM
Phenazine Methosulfate (PMS)	12.5 μM
Mg ²⁺ (MgCl ₂)	1 mM
PEG 8000	10% (w/v)

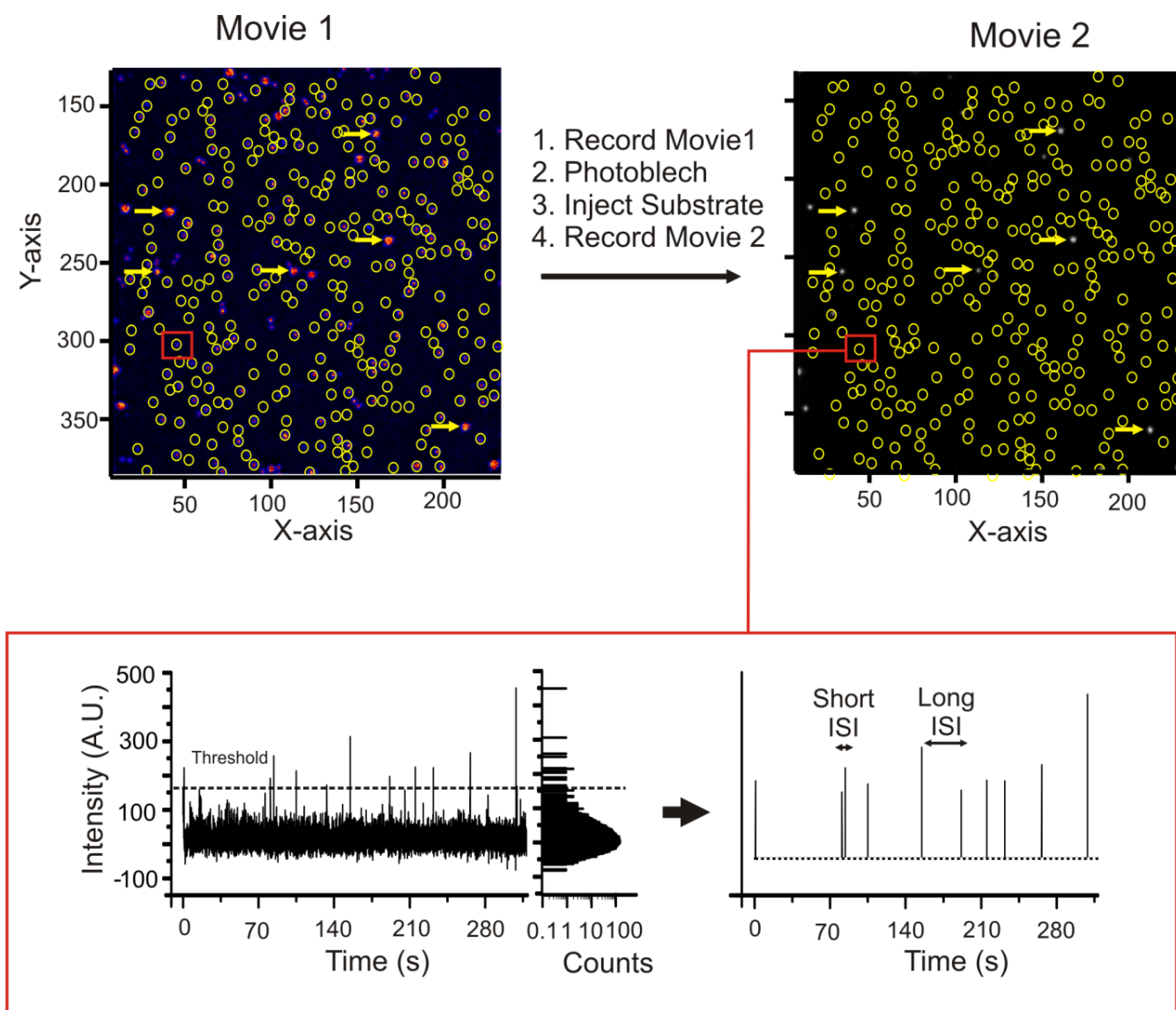


Fig. S27. Experimental workflow of the single molecule enzyme assay. Fluorescent beads (indicated by arrows) were used as fiduciary markers to correct for microscope slide/stage drift during the course of experiment. Enzyme activity of the G6pDH scaffolded tweezers (circles) were recorded in the same field of view after photobleaching the fluorophores. The enzyme activity movie (Movie 2) was registered with the initial movie (Movie 1) and the fluorescence-time traces were analyzed for inter-spike intervals (ISIs) at each tweezer location (bottom panel) after background correction (dotted line \approx mean intensity + $8 \times$ standard deviation, SD) using spike train analysis.

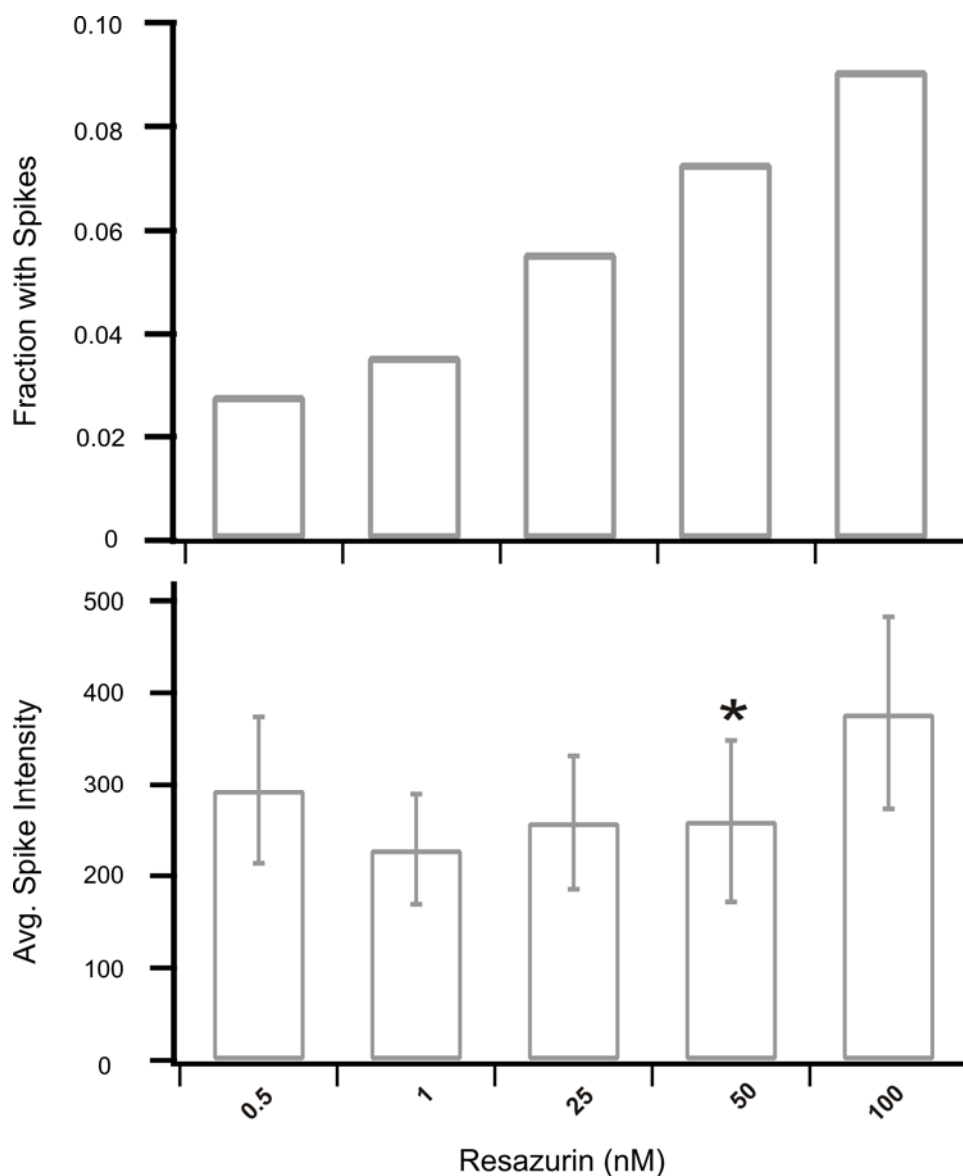


Fig. S28. Monitoring individual enzyme behavior at different concentrations of resazurin. (a) Fraction of molecules showing fluorescent spikes over the concentration range of 0.5-100 nM resazurin. As expected, a higher number of enzymes crosses our empirical intensity threshold so that the fraction of active enzymes increases with increasing concentration of resazurin (see Experimental). A decrease in ISI may also be expected at increasing concentrations of resorufin, however, the comparison of ISIs was not statistically reliable in this experiment as only few molecules were found to be active at low resazurin concentrations. (b) Spike intensity for the concentration range studied. The average intensity remains constant (within error) over the concentration range studied, suggesting that each spike represents a single catalytic turnover. The concentration of resazurin (50 nM) used for imaging single enzyme activities in this study is highlighted by an asterisk (*).

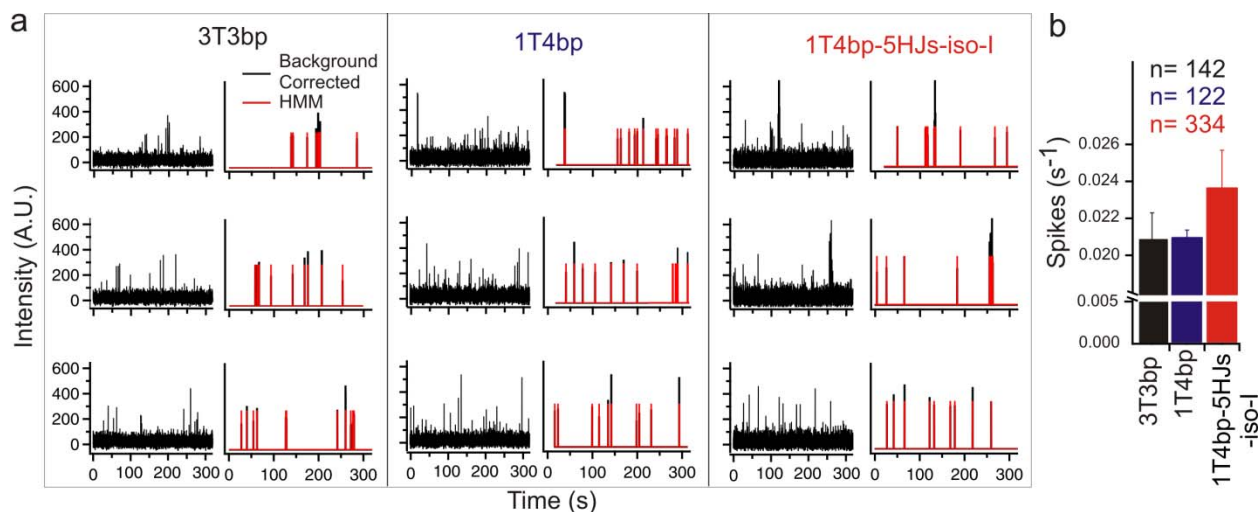


Fig. S29. Spike train analysis. (a) Representative fluorescence-time traces of three tweezer designs: 3T3bp, 1T4bp, and 1T4bp-5HJs-iso-I. The intensity-time traces (black) of tweezer-scaffolded G6pDH/NAD⁺ before and after background correction and Hidden Markov Model (HMM) idealization to a two-state model (red) are shown. The fluorescence intensity of enzyme reaction on the microscope slide was recorded for ~5 min at 35 ms time resolution. (b) Comparison of average spikes per molecule, where ‘n’ depicts the number of molecules analyzed (molecules with spikes above background, Fig. S27). The tweezer with redesigned HJs showed the highest spiking rate. All experiments were carried out at room temperature in 1× TBS buffer, pH 7.5 (Table S10).

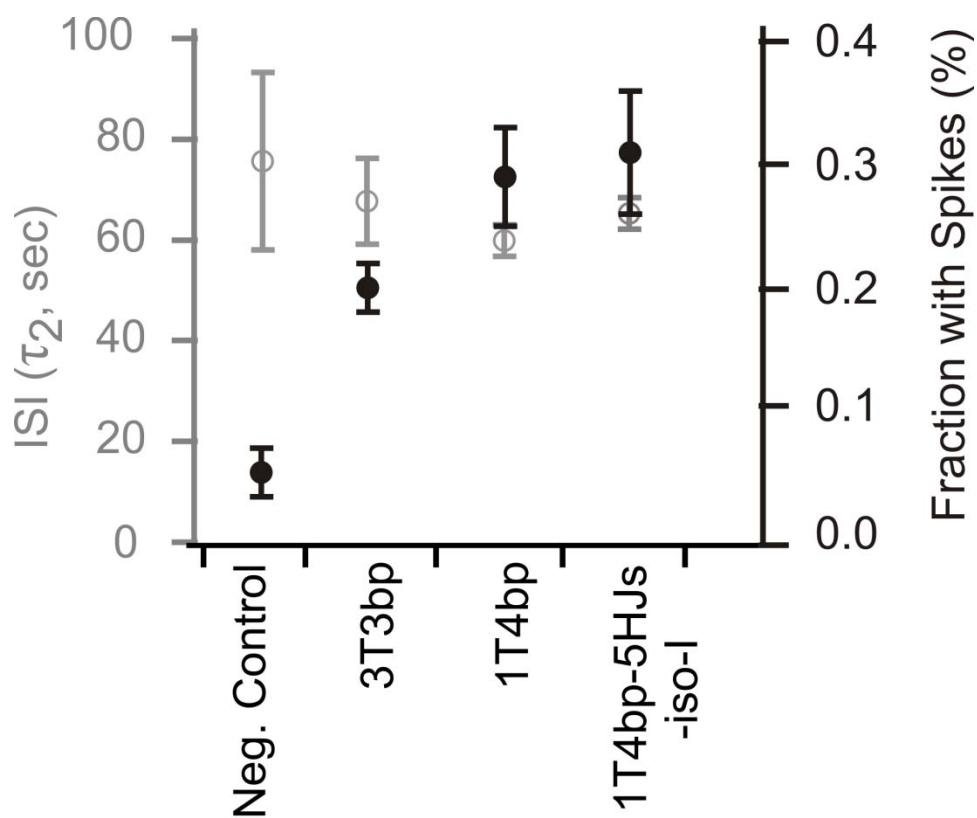


Fig. S30. Analysis of the long ISI (τ_2). According to our analysis, τ_2 reflects a less active conformational sub-state of the enzyme G6pDH. τ_2 values were obtained from the double-exponential fitting of the ISI data in Fig. 4e. While the average ISI values (gray, left axis) are only slightly shorter in the presence of substrate, the fraction of molecules showing spikes above background (black, right axis) is significantly higher in the presence of substrate compared to the negative control ((-)G6p) experiment.

References

- 1 N. C. Seeman and N. R. Kallenbach, *Biophys. J.*, 1983, **44**, 201-209.
- 2 J. Zheng, J. J. Birktoft, Y. Chen, T. Wang, R. Sha, P. E. Constantinou, S. L. Ginell, C. Mao and N. C. Seeman, *Nature*, 2009, **461**, 74-77.
- 3 N. Nguyen, J. J. Birktoft, R. Sha, T. Wang, J. Zheng, P. E. Constantinou, S. L. Ginell, Y. Chen, C. Mao and N. C. Seeman, *J. Mol. Recognit.*, 2012, **25**, 234-237.
- 4 M. Zuker, *Nucleic Acids Res.*, 2003, **31**, 3406-3415.
- 5 K. Pan, D.-N. Kim, F. Zhang, M. R. Adendorff, H. Yan and M. Bathe, *Nat. Commun.*, 2014, **5**, DOI: 10.1038/ncomms6578.
- 6 M. I. Wallace, L. Ying, S. Balasubramanian and D. Klenerman, *Proc. Natl. Acad. Sci.*, 2001, **98**, 5584-5589.
- 7 Y. Ke, S. M. Douglas, M. Liu, J. Sharma, A. Cheng, A. Leung, Y. Liu, W. M. Shih and H. Yan, *J. Am. Chem. Soc.*, 2009, **131**, 15903-15908.
- 8 N. Michaud-Agrawal, E. J. Denning, T. B. Woolf and O. Beckstein, *J. Chem. Phys.*, 2011, **32**, 2319-2327.
- 9 X.-J. Lu and W. K. Olson, *Nucleic Acids Res.*, 2003, **31**, 5108-5121.
- 10 X.-J. Lu and W. K. Olson, *Nat. Protoc.*, 2008, **3** 1213-1227.